Spatiotemporal regulation of *de novo* and salvage purine synthesis during brain development

Author: Tomoya Mizukoshi[1], Seiya Yamada[1]*, and Shin-ichi Sakakibara[1]*

Affiliation: [1]Laboratory for Molecular Neurobiology, Faculty of Human Sciences, Waseda University, Tokorozawa, Saitama, Japan.

*To whom correspondence should be addressed: Shin-ichi Sakakibara or Seiya Yamada, Laboratory for Molecular Neurobiology, Faculty of Human Sciences, Waseda University, Tokorozawa, Saitama 359-1192, Japan; sakakiba@waseda.jp or s.yamad@aoni.waseda.jp; tel. +81-4-2947-7120

Abstract

The levels of purines, essential molecules to sustain eukaryotic cell homeostasis, are regulated by the coordination of the *de novo* and salvage synthesis pathways. In the embryonic central nervous system (CNS), the *de novo* pathway is considered crucial to meet the requirements for the active proliferation of neural stem/progenitor cells (NSPCs). However, how these two pathways are balanced or separately utilized during CNS development remains poorly understood. In this study, we showed a dynamic shift in pathway utilization, with greater reliance on the *de novo* pathway during embryonic stages and on the salvage pathway at postnatal–adult stages. The pharmacological effects of various purine synthesis inhibitors *in vitro* and the expression profile of purine synthesis enzymes indicated that NSPCs in the embryonic cerebrum mainly utilize the *de novo* pathway. Simulatenously, NSPCs in the cerebellum require both the *de novo* and the salvage pathways. *In vivo* administration of *de novo* inhibitors resulted in severe hypoplasia of the forebrain cortical region, indicating a gradient of purine demand along the anteroposterior axis of the embryonic brain, with cortical areas of the dorsal forebrain having higher purine requirements than ventral or posterior areas such as the striatum and thalamus. This histological defect of the neocortex was accompanied by strong downregulation of the mechanistic target of rapamycin complex 1 (mTORC1)/ribosomal S6 kinase (S6K)/S6 signaling cascade, a crucial pathway for cell metabolism, growth, and survival. These findings indicate the importance of the spatiotemporal regulation of both purine pathways for mTORC1 signaling and proper brain development.

Introduction

The spatiotemporally regulated proliferation of neural stem cells and the migration of newborn neurons are crucial for forming the mammalian cerebral cortex. In the embryonic mouse brain, neural stem cells actively and symmetrically proliferate in the ventricular zone (VZ) to expand their original pool, eventually dividing asymmetrically to generate either intermediate progenitor cells (IPs) or neurons. Here, the neural stem cells in the VZ and the IPs in the subventricular zone (SVZ) are collectively referred to as neural stem/progenitor cells (NSPCs). Numerous glutamatergic neurons generated from NSPCs migrate radially to form the stratified layers of the cerebral cortex (Agirman et al., 2017). In addition, many GABAergic inhibitory neurons, generated in the embryonic ganglionic eminence (GE), tangentially migrate, finally integrating in the cerebral cortex (Lavdas et al., 1999; Cho et al., 2014; Corbin et al., 2003). Defects in radial migration frequently cause brain malformation and psychiatric disorders, including mental retardation and epilepsy (McManus and Golden, 2005).

Purines are the essential building blocks of DNA/RNA, energy sources of enzymatic reactions (ATP/GTP), and second messengers in various intracellular signaling cascades (cyclic AMP and cyclic GMP). Moreover, adenosine and ATP are involved in extracellular signaling mediated by purinergic receptors, regulating cell functions, such as cell migration, apoptosis, NSPC proliferation, and neuron differentiation (Huang et al., 2021, Lin et al., 2007).

There are two pathways for purine synthesis in mammals: the *de novo* and salvage pathways. In the latter, purines are synthesized by recycling degraded bases (AMP, GMP, and IMP) derived from the catabolism (Jurecka, 2009). The hypoxanthine-guanine phosphoribosyl transferase (HGPRT) converts hypoxanthine and guanine into inosine monophosphate (IMP) and guanine monophosphate (GMP), respectively,

whereas the adenine phosphoribosyltransferase synthesizes AMP from adenine (Fig 1A) (Pedley and Benkovic, 2017). Under physiological conditions, purines are generally supplied primarily via the salvage pathway. The *de novo* pathway is supposed to be set off when the demand for purines exceeds the capacity of salvage synthesis (Pareek et al., 2020). The *de novo* pathway produces IMP from phosphoribosyl-pyrophosphate through 10 consecutive reactions mediated by six enzymes [phosphoribosyl pyrophosphate amidotransferase, phosphoribosylglycinamide formyltransferase, formylglycin-amidine ribonucleotide synthase (FGAMS), phosphoribosylaminoimidazolecarboxylase phosphoribosyl-aminoimidazole succinocarboxamide synthetase (PAICS), adenylosuccinate lyase (ADSL), and 5-aminoimidazole-4-carboxamide ribonucleotide formyltransferase/IMP cyclohydrolase (ATIC)] (Fig 1A) (Pareek et al., 2021). These six *de novo* enzymes are assembled into a huge complex called purinosome, enabling a higher efficacy of IMP synthesis (An et al., 2008; French et al., 2016; Pedley and Benkovic, 2017). In fact, we recently demonstrated that a defect in purinosome formation leads to malformation of the cerebral cortex (Yamada et al., 2020). Other studies also provided evidence of a close relationship between purine production and the mTORC1 signaling pathway (Ben-Sahra et al., 2016; Hoxhaj et al., 2017), while the molecular interplay between the mTORC1 signaling and the purine metabolism in cortical development remains unclear.

Furthermore, abnormalities in the purine metabolism are associated with the etiology of many diseases, including gout. For instance, inherited deficiencies in *de novo* enzymes result in fetal lethality or neurological diseases in humans (Jurecka, 2009). For instance, a missense mutation in *PAICS* causes multiple malformations and early neonatal death (Pelet et al., 2019) and *ADSL* or *ATIC* deficiency causes various

neurodevelopmental phenotypes, including epilepsy, speech impairment, and auto-aggressive behavior (Marie et al., 2004; Jurecka et al., 2015; Dutto et al., 2022). With respect to the salvage pathway, *HGPRT* deficiency causes the Lesch-Nyhan syndrome, characterized by juvenile gout, dystonia, mental retardation, and compulsive self-injurious behavior (Lesch and Nyhan, 1964; Torres and Puig, 2007). Although *HGPRT* deficiency is thought to cause functional impairment of the dopamine system in the basal ganglia (Visser et al., 2000), no fundamental therapeutic approach has been established.

These previous studies strongly suggest that the balance between *de novo* and salvage purine synthesis pathways is critical for healthy brain development. However, the spatiotemporal regulation of purine production pathways in CNS development remains unknown. Here, we report the expression profile and the functional significance of purine synthesis enzymes in the developing brain. Each purine pathway is driven by its own temporal and regional traits during brain development.

Materials and Methods

Animals

ICR and C57BL/6J mice (Japan SLC Inc., Shizuoka, Japan) were housed under temperature- and humidity-controlled conditions on a 12/12 h light/dark cycle, with *ad libitum* access to food and water. The date of conception was established using a vaginal plug and recorded as embryonic day zero (E0.5). The day of birth was designated as P0. All protocols were approved by the Committee on the Ethics of Animal Experiments of Waseda University. Every effort was made to minimize mouse suffering.

Tissue preparation

Embryonic and adult mice were perfused through the cardiac ventricle with 4% paraformaldehyde (PFA) in 0.1 M phosphate buffer (pH 7.4), followed by post-fixation overnight at 4ºC (Yamada and Sakakibara, 2018). Fixed brains were cryoprotected in 30% sucrose in phosphate-buffered saline (PBS) overnight at 4°C and embedded in the optimal cutting temperature compound (Sakura Finetek, Tokyo, Japan). Frozen sections of embryonic and postnatal brains were cut into 14 μm thickness sections using a cryostat and collected on MAS-coated glass slides (Matsunami Glass, Osaka, Japan). Free-floating sections of adult mice brains were cut at 30 μm thickness.

Primary cell culture

NSPCs were cultured as described previously (Yamada and Sakakibara, 2018; Yumoto et al., 2013). They were first isolated from the E12.5 telencephalon or P2 external granular layer of the cerebellum, seeded onto dishes coated with 5 μg/mL fibronectin and 0.2% polyethyleneimine (Merck Millipore, Burlington, MA, USA), and cultured in Advanced DMEM/F-12 (1:1) (Thermo Fisher Scientific) supplemented with 15 μg/mL insulin (Thermo Fisher Scientific), 25 μg/mL transferrin (Thermo Fisher Scientific), 20 nM progesterone (Merck Millipore), 30 nM sodium selenite (Merck Millipore), 60 nM putrescine (Merck Millipore), 20 ng/mL fibroblast growth factor 2 (Merck Millipore), and 10 ng/mL epidermal growth factor (Merck Millipore). To assess cell proliferation, 10 μM 5-bromodeoxyuridine (BrdU) (Tokyo Chemical Industry, Tokyo, Japan) was administered to the cultured NSPCs. After 24 h of incubation, cells were cultivated in the medium without BrdU for the indicated periods and processed for immunostaining using an anti-BrdU antibody. Electroporation of Paics shRNAs into NSPCs was

performed as described previously (Yamada et al., 2020). The validated targeting sequences for Paics shRNA #1 and shRNA #3 were 5′-CTGCTCAGATATTTGGGTTAA-3′ and 5′-GCACCTGCTTTCAAATACTAT-3′, respectively (Yamada et al., 2020). The NSPCs expanded *in vitro* were electroporated with Paics shRNAs using a NEPA21 electroporator (Nepagene, Chiba, Japan) according to manufacturer's specifications (NSPCs: two pulses of 125 V for 5 ms with a 50 ms interval). After 96 h of culturing, cells were incubated with 10 μM BrdU for 24 h and fixed. To obtain primary cortical neurons (PCNs), E16.5 cerebral cortices or P4 cerebellar cortices were dissected and dispersed as previously described (Yamada et al., 2022). Cells were seeded onto poly-D-lysine-coated dishes (Merck Millipore) and cultured in a neurobasal medium containing 2% B27 (Thermo Fisher Scientific) and 1% GlutaMax (Thermo Fisher Scientific) for 10 days *in vitro* (div).

Immunohistochemistry

Immunohistochemistry (IHC) was performed as described previously (Yamada and Sakakibara, 2018). For antigen retrieval, frozen sections were heated at 90°C–95°C for 10 min in 10 mM sodium citrate buffer (pH 6.0) using a microwave and treated with 1% H_2O_2 in PBST (0.1% Triton X-100 in PBS) for 30 min at 20°C–25°C to suppress the endogenous peroxidase activity. Sections were blocked for 2 h in 10% normal goat serum in PBST and incubated overnight at 4°C with the primary antibodies in blocking buffer. Then, the sections were incubated with biotinylated anti-rabbit IgG (Vectastain ABC Elite; Vector Lab, Burlingame, CA) in PBST at room temperature for 2 h, followed by incubation with the ABC reagent (Vectastain ABC Elite; Vector Lab) in PBST for 2 h. The horseradish peroxidase signal was visualized using 2.25%

diaminobenzidine and 2.25% H_2O_2 (Peroxidase Stain DAB Kit; Nacalai tesque, Osaka, Japan). Each step was followed by four washes in PBST. Free-floating sections were mounted on MAS-coated glass slides, dehydrated, and coverslipped with Entellan New (Merck Millipore).

Double immunostaining was performed as described previously (Yamada and Sakakibara, 2018; Yamada et al., 2020). Frozen sections were blocked for 2 h with 5% normal goat or donkey serum in PBST, followed by incubation with the primary antibodies in blocking buffer at 4°C overnight. After washing with PBST four times and twice with PBS, sections were incubated for 2 h with Alexa Fluor 488- or Alexa Fluor 555- conjugated secondary antibodies (Thermo Fisher Scientific). After counterstaining with 0.7 nM Hoechst 33342 (Thermo Fisher Scientific), sections were mounted and imaged using a confocal (FV3000, Olympus) or fluorescence inverted microscope (Axio Observer, Zeiss). For BrdU staining, sections were treated with 2 N HCl for 30 min at 42°C for DNA denaturation, followed by treatment with 0.1 M sodium borate buffer (pH 8.5) for 10 min. fter washing with PBST four times and twice with PBS, anti-BrdU immunostaining was performed.

Immunocytochemistry

Cultured cells were fixed with 4% PFA and permeabilized with 0.1% Triton X-100. For BrdU staining, cells were treated with 2 N HCl for 1 h at 37°C, followed by neutralization with 0.1 M sodium borate buffer (pH 8.5) for 30 min. After blocking with 5% normal donkey serum, cells were incubated with primary antibody for 1 h at room temperature, followed by Alexa Fluor 488- or 594-conjugated secondary antibodies (Thermo Fisher Scientific) for 2 h. Immunofluorescent signals were acquired using an

inverted microscope (Axio Observer, Zeiss) equipped with a CCD camera (AxioCam MRm, Zeiss).

Primary antibodies

The following antibodies were used: anti-α-tubulin (rabbit polyclonal, #11224-1-AP, Proteintech; 1:5000 for Western blot, WB), anti-PAICS (rabbit polyclonal, #12967-1-AP, Proteintech; 1:1500 for WB, 1:200 for IHC), anti-PFAS (FGAMS) (rabbit polyclonal, #A304-218A, Bethyl Lab; 1:1500 for WB, 1:200 for IHC), anti-HPRT1 (rabbit polyclonal, #15059-1-AP, Proteintech; 1:3000 for WB, 1:1000 for IHC), anti-Pax6 (rabbit polyclonal, #PD022, MBL; 1:3000 for WB), anti-CD31 (rat monoclonal clone ER-MP12, #MCA2388T, BioRad Laboratory; 1:200 for IHC), anti-Nestin (chicken polyclonal, #GTX85457, Gene Tex; 1:1500 for ICC), anti-BrdU (sheep polyclonal, #ab1893, Abcam, 1:1500 for IHC and ICC), anti-Ki67 (rabbit monoclonal clone SP6, #RM-9106, Lab Vision; 1:1000 for IHC), anti-Phospho-Histone H3 (Ser10) (mouse monoclonal clone 6G3, #9706, Cell Signaling Technology; 1:1000 for IHC), anti-p70 S6K (Thr389) (108D2) (rabbit monoclonal, #9234, Cell Signaling Technology; 1:1000 for WB), anti-p70 S6K α (mouse monoclonal clone H-9, #sc-8418, Santa Cruz Biotechnology; 1:1000 for WB), anti-pS6 ribosomal protein (Ser240/244) (rabbit polyclonal, #2215, Cell Signaling Technology; 1:1000 for WB), anti-S6 ribosomal protein (mouse monoclonal clone C-8, #sc-74459, Santa Cruz Biotechnology; 1:1000 for WB), anti-4E-BP1 (rabbit monoclonal clone 53H11, #9644, Cell Signaling Technology; 1:1000 for WB), and anti-GSH2 (rabbit polyclonal, #ABN162, Sigma Aldrich; 1:200 for IHC).

Drugs

The following drugs were used: mycophenolate mofetil (MMF) (#S1501, Selleck, 100 mg/kg *in vivo*, 1–10 μM *in vitro*, dissolved in DMSO), methotrexate (MTX) (#139-13571, Fujifilm Wako, 50 mg/kg *in vivo*, 1–100 μM *in vitro*, dissolved in Na_2CO_3), forodesine hydrochloride (#HY-16209, MCE, 40 mg/kg *in vivo*, 0.1–5 μM *in vitro*, dissolved in PBS), allopurinol (#17795-21-0, Selleck, 50 mg/kg *in vivo*, 250 μM i*n vitro*, dissolved in DMSO), BrdU (#B1575, Tokyo Chemical Industry, 100 mg/kg *in vivo*, 10 μM *in vitro*, dissolved in PBS). For *in vitro* culture, drugs were added to the medium at the indicated concentration and incubated for 48 h. BrdU was added 24 h prior to fixation to mark S-phase cells. For *in vivo* experiments, the inhibitor was administered to pregnant dams or postnatal pups by a single intraperitoneal injection (i.p.) at E12.5, E16.5, or P2, followed by BrdU injection at E13.5, E17.5, or P4, respectively. Embryos or pups were fixed at E14.5, E18.5, or P6 in each condition. In some experiments, the inhibitor was injected daily into pregnant mice from E9.5 to E11.5, and the fetuses were fixed at E12.5.

Western blotting

Tissue lysates were prepared by homogenization in RIPA buffer [25 mM Tris–HCl (pH 7.6), 150 mM NaCl, 1% NP40, 1% sodium deoxycholate, 0.1% sodium dodecyl sulfate, containing protease inhibitors (cOmplete Mini Protease Inhibitor Cocktail, Sigma Aldrich)], followed by centrifugation at 15,000 rpm for 10 min. Western blotting was performed as described previously (Yamada et al., 2020). For pS6 and pS6K detection, the membranes were blocked using 1% bovine serum albumin (BSA) fraction V (Fujifilm Wako) in 0.1% Tween 20 in Tris-buffered saline (TBST), followed by

incubation with a primary antibody diluted by 1% BSA in TBST.

Statistical analyses

Statistical analyses were performed using the R package version 4.2.0. All numerical data are expressed as mean ± SEM. A one-way ANOVA followed by Weltch's t-test with Holm–Bonferroni correction was used in multiple-group comparisons. Welch's t-test was used to assess the number of $BrdU^+$ or $pH3^+$ cells *in vivo* and pS6/S6 ratio. In *in vivo* experiments involving inhibitors, three individuals were tested per condition and three images from each individual were randomly selected for statistical processing. The chi-squared test was used to compare the number of $BrdU^+$ $Nestin^+$ cells *in vitro*. *, $P < 0.05$; **, $P < 0.01$; ***, $P <0.001$ were considered statistically significant. The number of $BrdU^+$ NSPCs *in vitro* was counted using MATLAB [version 9.12.0.1884302 (R2022a)].

Results

Two purine synthesis pathways are activated during brain development

To investigate the expression of purine synthesis enzymes in the developing CNS, immunoblotting analysis was performed on embryonic, postnatal, and adult brains. PAICS and FGAMS, both catalyzing the *de novo* purine synthesis (Fig. 1A), were abundant in the embryonic stages from E10.5 to E16.5, during the active NSPC proliferation. Subsequently, from the postnatal to the adult stage, the expression of these *de novo* enzymes was downregulated (Fig. 1B). Conversely, the expression of HGPRT, a key enzyme catalyzing the salvage pathway (Fig. 1A), was relatively low in embryonic brains, gradually increasing in postnatal and adult stages (Fig. 1B). Although

HGPRT was expressed as a 25 kDa product with the expected size throughout life, an additional product of 35 kDa was detected during the embryonic and neonatal (E13–P0) period. Whether this slower-migrating band reflects another isoform or a post-translationally modified HGPRT product is unclear. We next analyzed the expression of these enzymes in primary cultured NSPCs isolated from E12.5 cerebral cortices and the external granular layer (EGL) of the P2 cerebellum. Figure 1C shows that PAICS and FGAMS were abundantly expressed in NSPCs derived from these two brain regions. In contrast, PAICS and FGAMS expression was decreased in PCNs (Fig. 1C) isolated from E16.5 cerebral or P4 cerebellar cortices and cultured for 10 divisions until fully differentiated. These observations appear consistent with the *in vivo* expression profile of FGAMS and PAICS along brain development (Fig. 1B). On the other hand, HGPRT was expressed in cultured NSPCs as well as the PCNs (Fig. 1C). The purity of the NSPCs used in this assay was confirmed by the expression of Pax6, a marker for embryonic apical progenitor cells/radial glial cells (RGCs) (Fig. 1C). In the cerebellum, the Pax6 protein is expressed in differentiated granular cells as well as cerebellar NSPCs (Yamasaki et al., 2001). Consistently, we detected Pax6 in PCNs derived from the cerebellar EGL (Fig. 1C). These results suggested that the *de novo* pathway is preferentially driven during the embryonic stage when NSPC proliferation occurs, and that purine metabolism switches from the *de novo* pathway to the salvage pathway over brain development.

Expression of purine synthesis enzymes in the developing and adult CNS

The distribution and localization of PAICS, FGAMS, and HGPRT were examined immunohistochemically in the developing and matured mouse brain. At E13.5, three

enzymes were strongly expressed in the VZ/SVZ of the cerebral cortex, where NSPCs localize (Fig. 2A–C). These immunoreactivities in the VZ/SVZ considerably decreased until E18.5 and P0 (Fig. 2A–F, J–L), decreasing until disappearing in the SVZ of the adult cerebral cortex (Fig. 2P–R). The development of the cerebellum proceeds rapidly from late embryonic stages. Granule neurons are produced from NSPCs in the superficial EGL covering the cerebellar cortex and migrate to form the internal granule layer (IGL) (Yacubova & Komuro, 2003). We observed robust HGPRT immunoreactivity in the EGL at E18.5 and P0; meanwhile, the PAICS and FGAMS expression level in the EGL was relatively weak (Fig. 2G–I, M–O, arrows). These observations might indicate that embryonic NSPCs actively drive purine synthesis pathways to meet the high demand at the beginning; as neurogenesis progresses though, the activity of the purine synthesis pathway would decline. We further detected HGPRT expression in $CD31^{+}$ endothelial cells of blood vessels in the brain parenchyma from E13.5 to P0.5 (Figs. 2S, S1A, B), but HGPRT was not observed in blood vessels in the adult brain. These results suggested a specific role of the salvage pathway in vasculogenesis in the embryonic brain.

In the adult brain, PAICS, FGAMS, and HGPRT were widely detected in neuronal somata and neuropil of discrete areas (Figs. S2 and S3). In the brain stem, the locus coeruleus, Edinger-Westphal nucleus, and vestibular nucleus expressed these three enzymes. Moreover, strong immunoreactivities for PAICS and FGAMS were differentially observed in several nuclei of the brain stem, including the lateral cerebellar, red, facial, medial vestibular, and ambiguous nucleus (Figs. S2 and S3). On the other hand, HGPRT was preferentially expressed in numerous nuclei in the forebrain and diencephalon, including the posterior interlaminar thalamic nucleus, polymorph

layer of the dentate gyrus, arcuate nucleus, dorsomedial hypothalamic nucleus, zona incerta, lateral septal nuclei, and neurons in the nigrostriatal bundle (Figs. S2 and S3). These findings implied that the purine pathway to be activated depends on the developmental stage and brain region involved.

Inhibiting *de novo* purine synthesis affects NSPC proliferation

We sought to investigate the effects on brain development of purine synthesis inhibition during a specific period in embryonic and postnatal life. To this end, using genetically engineered animals, such as knockout mice and conditional knockout mice of purine synthesis enzymes, was limited in their ability to transiently suppress the enzyme activity in the mid or late embryonic period, times of active neurogenesis in the cerebral cortex. In this study, we used several inhibitors that target specific enzymes of purine synthesis pathways. These inhibitors allowed us to target a specific embryonic period and to easily adjust the degree of inhibition during corticogenesis depending on inhibitor concentration.

First, the role of purine pathways in NSPCs was explored using various specific inhibitors for the *de novo* and salvage enzymes. Accordingly, primary cultured NSPCs prepared from E12.5 cerebral cortex were incubated for 48 h with or without the following inhibitors (Fig. 1A): MMF, an inhibitor of the inosine monophosphate dehydrogenase, which is the rate-limiting enzyme in *de novo* synthesis of guanosine nucleotides (Allison, 2005) or forodesine hydrochloride, an inhibitor of the purine nucleoside phosphorylase mediating the salvage pathway (Evans et al., 2018). Immunostaining with anti-Nestin, an NSPC marker and anti-BrdU revealed that MMF treatment significantly reduced the number of Nestin^{+} BrdU^{+} NSPCs, while forodesine

treatment did not affect NSPC proliferation (Fig. 3A–D). With MMF treatment, no morphological changes or enhanced differentiation into neurons were observed in Nestin^{+} NSPCs, suggesting that MMF exclusively affected the mitotic potential of NSPCs. Similar results were obtained in the NSPCs isolated from the cerebellar EGL (Fig. S4A–D). Next, we confirmed that the reduced NSPC proliferation was caused by repression of the *de novo* pathway using PAICS shRNAs. The silencing effect and specificity of PAICS shRNAs (#1 and #3) were validated in our previous study (Yamada et al., 2020). Consistent with the inhibitory effect of MMF on NSPC division, knocking down *PAICS* significantly decreased the number of BrdU-incorporated NSPCs (Paics shRNA #1, 37%, n = 100; Paics shRNA #3, 6%, n = 100, arrows) relative to the control (control shRNA, 67%, n = 100, arrowhead) (Fig. 3E–G). Based on these results, we concluded that activation of the *de novo* pathway is critical for NSPC proliferation.

The development of the cerebellum requires both purine synthesis pathways

Next, we examined the significance of the purine pathways on *in vivo* neurogenesis in the cerebellum. To this end, embryos at E16.5 or pups at P2 mice were treated with forodesine, MMF, or MTX. MTX is known to impede the *de novo* purine pathway at multiple steps by inhibiting the dihydrofolate reductase, which catalyzes the folate biosynthesis pathway (Fig. 1A) (Cronstein, 1997). Gross anatomical analysis two or four days after inhibitor administration showed no significant brain dysplasia. However, immunostaining with BrdU and Ki67, which marks cells with proliferative capacity, showed that the fraction of BrdU^{+} and Ki67^{-} cells increased in the E18.5 cerebellar IGL treated with forodesine, MMF, and MTX compared with control (Fig. 4A–E) (control,

20.6 ± 2.7%, n = 7; forodesine, 40.3 ± 2.7%, n = 8; MMF, 34.4 ± 2.9%, n = 7; MTX, 49.6 ± 3.2%, n = 9). Comparable results were observed in the P6 cerebellar IGL treated with forodesine or MMF (Fig. 4F–I) (control, 27.1 ± 1.5%, n = 9; Forodesine, 38.4 ± 3.2%, n = 7; MMF, 42.8 ± 2.7%, n = 9). These findings suggest that inhibition of purine synthesis in the cerebellum may accelerate the exit from the cell cycle in NSPCs, affecting cell fate determination and leading to impaired cerebellar development. Considering the abundant HGPRT expression in EGL (Fig. 2I, O), proper development of the cerebellum requires the salvage as well as the *de novo* pathways.

MMF suppresses NSPC proliferation and delays neuron migration in the cerebral cortex

To assess the impact of the purine pathway on neurogenesis in the embryonic cerebral cortex, MMF or forodesine was administered at E12.5, followed by BrdU administration at E13.5, and embryo analysis at E14.5. In the control, many BrdU-incorporated NSPCs exited the cell cycle and left the SVZ/VZ; about half of $BrdU^+$ cells were dispersed within the intermediate zone (IZ) and cortical plate (CP) at E14.5 (Fig. 5A, D) (CP, 8.2 ± 1.1%; IZ, 42.9 ± 2.0%; SVZ/VZ, 48.9 ± 1.3%, n = 9). In contrast, MMF-treated embryos exhibited a substantial accumulation of $BrdU^+$ cells in the SVZ/VZ, with few $BrdU^+$ cells being located in the IZ/CP (Fig. 5C, D) (CP, 0.1 ± 0.1%; IZ, 27.7 ± 3.5%; SVZ/VZ, 72.2 ± 3.5%, n = 9), indicating suppression of radial migration of newborn neurons. On the other hand, forodesine treatment had only a small effect on neuron migration (Fig. 5B, D) (CP, 2.5 ± 0.8%; IZ, 40.4 ± 3.1%; SVZ/VZ, 57.1 ± 3.1%, n = 9). To determine whether the $BrdU^+$ cells remaining in the VZ/SVZ had lost their mitotic potential, we performed immunostaining with an antibody to

phospho-histone H3 (pH3), which marks cells in late G2-M phase. Compared to controls, the number of $pH3^+$ NSPCs in the VZ facing the lateral ventricles was significantly reduced in MMF-treated embryos (Fig. 5E, G, H, arrows) (control, 31.1 ± 3.5, n = 11; MMF, 19.0 ± 1.4%, n = 9). Meanwhile, the number of $pH3^+$ NSPCs in the VZ remained unchanged in forodesine-treated embryos (Fig. 5F, H) (34.2 ± 1.9%, n = 9). Immunostaining with anti-PAICS, FGAMS, and HGPRT showed that the expression and subcellular localization of each enzyme were not affected by treatment with these inhibitors, as all these enzymes were expressed in the cytoplasm in the VZ/SVZ (Fig. 5I–Q). These results suggested that inhibition of the *de novo* pathway, but not of the salvage pathway, suppressed NSPC mitosis and the subsequent neuron migration from the VZ.

Inhibiting *de novo* pathway causes forebrain-specific malformations

To investigate the effect of prolonged inhibition of the purine pathway, embryos continuously received each inhibitor (MMF, forodesine, MTX, allopurinol, or MTX and allopurinol) from E9.5 to E11.5; their brain architecture was analyzed at E12.5. Allopurinol is an inhibitor of the xanthine oxidase, which converts xanthine to uric acid which can rescue purine synthesis via the salvage pathway (Fig. 1A) (Day et al., 2017). In our study, embryos treated with forodesine or allopurinol appeared to follow normal brain development (Figs. 6A, C, D, S5). On the other hand, a drastic anomaly was reproducibly observed in MMF-treated brains, in which the lateral ventricles widely opened into the third ventricle, probably due to forebrain hypoplasia (Fig. 6B). MTX-treated embryos did exhibit a more severe malformation, with complete loss of the forebrain region (Fig. 6E, E'). Co-treatment with MTX and allopurinol, which enhances

the salvage pathway, could not restore this effect (Fig. 6F). These observations further supported that the *de novo* purine synthesis pathway is predominantly involved in the development of the cerebral cortex, as the *de novo* synthesis inhibition impacted forebrain formation in early neural development.

To gain insights into the brain abnormality caused by the suppression of *de novo* purine synthesis, we performed a detailed histological analysis. As shown in Figure 7, MMF-treated embryos showed a significant increase of cleaved caspase3^{+} apoptotic cells in the rostral region of the cerebral cortex (area 1 in Fig. 7B), whereas a much lower number of apoptotic cells were detected in the caudal forebrain region (area 2). (Fig. 7A, B, Y) (control, 7.2 ± 1.2, n = 4; MMF area 1, 47.3 ± 7.7, n = 8; MMF area 2, 18.8 ± 2.7, n = 8). Neither the continuous inhibition of the salvage pathway by forodesine nor the activation of the salvage pathway by allopurinol had any effect on brain formation. In addition, forodesine treatment did not affect cell death (Fig. 7. C, Y) (16.4 ± 2.2, n = 6). Interestingly, allopurinol treatment resulted in a marked increase in the number of apoptotic cleaved-caspase3^{+} cells throughout the cerebral cortex (Fig. 7D, Y) (42.9 ± 5.6, n = 9).

Next, we performed double immunostaining with anti-Pax6 and anti-DCX, specific markers for RGCs in the cerebral cortex and postmitotic newborn neurons, respectively. The embryonic forebrain typically contains a VZ occupied by Pax6^{+} NSPCs and an IZ/CP occupied by DCX^{+} neurons, as shown in the DMSO-treated control. The structure of the embryonic forebrain treated with forodesine or allopurinol was equivalent to that of the control brain, and the spatial distribution of the two cell populations (Pax6^{+} NSPCs and DCX^{+} neurons) appeared unchanged (Fig. 7E, G, H). In contrast, in the forebrain of MMF-treated embryos, the distribution of Pax6- and DCX-

expressing cells was disrupted and drastically affected: Pax6 expression remained in the caudal area of the forebrain (area 2) but was completely absent in the rostral and dorsal parts (area 1; Fig. 7F). With respect to DCX^+ neurons, although their distribution was relatively preserved throughout the forebrain, the DCX^+ cortical layer was significantly expanded and thickened at the boundary between areas 1 and 2 (Fig. 7F, asterisk). Furthermore, the expression of T-box brain protein 2 (Tbr2) (Englund et al., 2005), an IP marker in the SVZ, was lost in area 1 of MMF-treated embryos, similar to Pax6 (Fig. 7I–L). Nonetheless, the number and distribution of $Ki67^+$ or $pH3^+$ proliferating cells in area 1 were unaffected (Fig. 7M–T, Z) (control, 32.7 ± 3.0, n = 4; MMF area1, 27.9 ± 1.6, n = 8; MMF area2, 27.3 ± 1.8, n = 8; forodesine, 25.9 ± 1.8, n = 6; allopurinol, 24.6 ± 3.1, n = 9). Immunostaining with Nestin, a universal RGC marker in all brain regions, unexpectedly revealed that $Nestin^+$ RGCs were uniformly distributed in areas 1 and 2 in MMF-treated brains. Since area 1 contains $Nestin^+$ but $Pax6^-$ RGCs we considered that maybe area 1 corresponds to a non-neocortical region that contains a different subtype of NSPCs. Previous studies have shown that Pax6 and Tbr2 are expressed in NSPCs of the embryonic cerebral neocortex, while GSH2, another homeobox gene, is specifically expressed in the NSPC population residing in lateral GE, representing the striatal primordium (Englund et al., 2005; Yun et al., 2001; Corbin et al., 2003). In fact, immunostaining MMF-treated brains with an anti-GSH2 antibody revealed that GSH2 was exclusively expressed in area 1, suggesting that area 1 is a structure derived from the lateral GE (Fig. 7W, X).

These histological analyses suggested that loss or hypoplasia of the rostral neocortex in MMF-treated brains may have caused dorsal displacement and bulging of ventral forebrain regions, including the striatal GE, resulting in abnormal forebrain-like

structures (Fig. 7AA). Consistent with the results in cultured NSPCs, these findings strongly suggest that the NSPC population in dorsal forebrain regions, such as the neocortex, is more susceptible to deficits in the *de novo* pathway than other brain regions. The large number of caspase3^{+} apoptotic cells in the GE-derived region of area 1 (Fig. 7B) also reflect a shift in dependence on the *de novo* pathway along the anteroposterior and dorsoventral brain axis.

De novo purine pathway controls mTORC1/S6K/S6 signaling

We attempted to elucidate the molecular mechanism by which the *de novo* purine pathway regulates cortical development. Among the various intracellular signaling pathways, we focused on the mammalian/mechanistic target of rapamycin (mTOR), a serine/threonine kinase involved in cell proliferation and growth through the regulation of numerous cellular processes (Szwed et al., 2021). Previous studies have shown that mTOR Complex 1 (mTORC1) stimulates purine nucleotides production (Ben-Sahra et al., 2016) and the inhibitory effect of purine nucleotide depletion on mTORC1 signaling (Hoxhaj et al., 2017). In addition, mTOR1 mutation affects the development of the cerebrum, suggesting a role for mTORC1 signaling in NSPCs (Tarkowski et al., 2019; Andrews et al., 2020). mTORC1 includes two downstream cascades, eukaryotic initiation factor 4E (eIF4E)/binding protein 1 (4E-BP1)and S6K/S6 (Fig. 8C) (Ben-Sahra et al., 2016; Morita et al., 2013). However, the molecular interplay between the two mTORC1 signaling cascades and the purine metabolism in cortical development remains unclear.

Brain lysates were prepared from E12.5 embryos continuously treated with MTX, allopurinol, or MTX plus allopurinol, and the expression levels of the downstream

proteins of mTORC1 signaling were examined. For the S6K/S6 signaling cascade, we analyzed the protein levels of ribosomal protein S6 kinase (S6K), phosphorylated S6K (pS6K), ribosomal protein S6 (S6), and phosphorylated S6 (pS6). As shown in Figure 8A, pS6K, S6K, and pS6 expression was completely abolished upon MTX treatment. Compared to controls, the S6 protein level was unchanged in MTX-treated brains, indicating that MTX completely inhibits S6 phosphorylation and activation in te embryonic brains (Fig. 8B). These MTX-induced severe impairments of the S6K/S6 signaling cascade were restored by the concurrent administration of allopurinol and MTX (Fig. 8A), which eventually restored the phosphorylation level of S6 to comparable levels as control (Fig. 8B). An immunoblot of eIF4E/4E-BP1 showed that 4E-BP1 was detected with a slightly lower molecular weight in MTX-treated brains, consistent with previous reports in cancer cells (Hoxhaj et al., 2017). However, a quantitative analysis showed no differences in the amount of 4E-BP1 protein (Fig. 8A).

These results indicate that the dorsal forebrain malformation caused by inhibition of the *de novo* purine synthesis was associated with mTORC1/S6K/S6 signaling but not with mTORC1/4E-BP1/eIF4E. Since activation of the salvage pathway by allopurinol restored the decreased mTORC1/S6K/S6 signaling, we consider that a steady state level of purines supplied by the *de novo* pathway is essential for the maintenance of mTORC1/S6K/S6 signaling within NSPCs in this brain region.

Discussion

Purine synthesis pathways are activated during brain development

We revealed that PAICS and FGAMS, two *de novo* purine synthesis enzymes, were abundant in the embryonic brain and downregulated toward postnatal and adult stages.

On the other hand, HGPRT, which promotes the salvage pathway, exhibited the opposite trend during brain development. These results indicates a switch in the main pathway of purine synthesis from the *de novo* pathway to the salvage pathway during brain development. This switch probably reflects that the *de novo* pathway is driven to meet the massive purine demand caused by active cell proliferation during the embryonic period, and that the salvage pathway becomes dominant after birth, when the energy cost stabilizes after the peak of neurogenesis and the demand for intracellular purines is reduced. Recent studies have indicated the presence of highly vascularized and avascular regions in the developing neocortex and that the nervous system and the vasculature of the brain are closely associated during the development of the cerebral cortex (Komabayashi-Suzuki et al., 2019). An avascular region forms on the VZ from E12.5 to E17.5, where dividing undifferentiated RGCs remain in contact with sprouting neovascular tip cells, which gradually shrinks over development (Bjornsson et al., 2015; Komabayashi-Suzuki et al., 2019). This avascular hypoxic niche is supposedly required to maintain the stemness of NSPCs as well as stem cells in other developing organs (Bjornsson et al., 2015; Komabayashi-Suzuki et al., 2019).

As the embryonic NSPCs in the VZ avascular region cannot receive sufficient purines or purine metabolites through blood vessels, it seems logical that NSPCs are strongly dependent on the *de novo* pathway during cortical development. Meanwhile, HGPRT is expressed in $CD31^{+}$ blood vessels during angiogenesis at embryonic stages; a colocalization not observed at the adult stage (Fig. 2S, S1). Thus, the salvage pathway in vascular endothelial cells may supply purines to the surrounding differentiating and migrating cells in the IZ/CP.

In the developing cerebellum, both *de novo* and salvage inhibitors affected the

proliferation of granular cells, indicating an essential role of both pathways in cerebellar development. One possible reason is that the *de novo* pathway alone may not be sufficient to supply purines since cerebellar NSPCs require large amounts of purines to undergo numerous symmetric cell divisions. Another possible reason is that the cerebellar NSPCs, located in the EGL, could drive the salvage pathway by receiving a supply of purine metabolites from the blood vessels of the meninges covering the brain surface. Over the past decade, a link between purine synthesis pathways and various cancers has been demonstrated (Di Virgilio & Adinolfi, 2017; Yin et al., 2018). In general, the intracellular concentration of purine metabolites and the activity of the de novo pathway enzymes are enhanced in cancer cells. Changes in the ratio of purine metabolites in tumor cells affect tumor growth, invasion, and metastasis. A switch in purine synthesis pathways that depends on the extracellular environment may not only exist in NSPCs but also in cancer stem cells and other tissue stem cells. This possibility could provide a valuable perspective for anticancer drug development.

Different purine synthesis pathway dependence of NSPCs according to brain regions

The immunohistochemical analysis of adult mouse brains indicated different dominant purine synthesis pathway according to brain region (Fig. S2, 3). In addition, this study showed that NSPCs have a different predominance of purine synthesis pathways depending on the brain region. The inhibition of *de novo* purine synthesis by drugs *in vivo* caused proliferation defects in NSPCs and delayed the migration of immature neurons in the embryonic neocortex. Accordingly, disturbance or loss of Pax6, Tbr2, and DCX expression in the neocortex was accompanied by a cortical malformation in

which Gsh2^{+} GE cells emerged in the dorsal forebrain region. The purine demand in NSPCs likely differs between the dorsal (cerebral neocortex) and ventral forebrain (GE). Considering that NSPCs in the neocortex and GE produce predominantly glutamatergic excitatory and GABAergic inhibitory neurons, respectively, the different cell lineage of each NSPC may explain the differences in the requirement of *de novo* purine synthesis. Indeed, we observed that cell death widely occurred in cells, including neurons in the CP in the rostral GE-like structures formed in MMF-treated embryos (Fig. 7B), implicating that the cells in GE-like structures are in distinct cell lineages from their surrounding structures. The reason why there is higher *de novo* purine production in the neocortex than other brain regions is still unclear. However, there may be a relationship between purine synthesis pathways and the evolution of mammals with a huge neocortex.

The *de novo* purine synthesis is involved in cortical formation through mTOR signaling

Our results indicated that inhibiting *de novo* purine synthesis by MMF or MTX during corticogenesis *in vivo* results in brain malformation. Clinical case reports indicate that prenatal exposure to MTX leads to fetal death or fetal MTX syndrome, which is characterized by CNS anomalies, including alobar holoprosencephaly (Corona-Rivera et al., 2010; Seidahmed et al., 2006). However, the molecular mechanism underlying the brain abnormalities induced by MTX remains unknown. We revealed that the brain malformation caused by inhibiting *de novo* purine synthesis was accompanied by a defect in mTORC1/S6K/S6 signaling. Our results are consistent with previous studies showing that inhibition of purine synthesis in tumor cells suppresses mTORC1/S6K/S6

signaling but not mTORC1/4E-BP1/eIF4E signaling (Emmanuel et al., 2017; Hoxhaj et al., 2017).

mTORC1 functions as a sensor for nutrients, energy, and redox status, regulating protein synthesis (Ben-Sahra et al., 2016; Hoxhaj et al., 2017). Particularly, mTORC1/S6K/S6 signaling cascade plays an essential role in regulation of protein translation. mTORC1 phosphorylates S6K, which in turn phosphorylates various substrate proteins, including ribosomal subunit S6, thereby promoting translation. Some patients with cortical malformations, such as hemimegalencephaly and focal cortical dysplasia, have been shown to carry mutations in *mTOR* (Tarkowski et al., 2019). Deficiency in *mTOR* causes morphological abnormalities in the brain, including a thinner cerebral cortex due to suppressed NSPC proliferation (Ka et al., 2014), suggesting a close correlation between the mTOR pathway and disruption of cortical development. These findings further supported our notion that *de novo* purine synthesis and the mTORC1/S6K/S6 signaling pathway tightly regulate each other spatiotemporally to control neocortical development.

Limitations of this study

In this study, we revealed a switch from *de novo* to salvage purine synthesis as brain development proceeds, and the *de novo* pathway plays a vital role in early embryonic corticogenesis, cooperating with the mTOR signaling pathway. We indicated the possibility that purine sensibility or predominance of purine synthesis pathways differ in NSPCs depending on the brain region. However, we could not clarify the molecular mechanisms of brain malformation by *de novo* purine synthesis inhibitors. Our future study would reveal regional and lineage-specific differences in purine metabolism in the

brain, which might shed light on the significance of adaptive changes in purine metabolic pathways during the evolution of the mammalian brain.

Declaration of competing interest

The authors declare no conflicts of interest or financial interests.

Acknowledgments

We would like to thank enago (www.enago.com) for English language editing.

Funding

This work was funded by the Japan Society for the Promotion of Science grants-in-aid (KAKENHI) grant numbers 21K20701 (to S.Y.) and 19K06931 (to S.S.), Gout and Uric Acid Research Foundation 2020 (to S. S) and 2022 (to S.Y.), and Waseda University Grants for Special Research Projects 2021C-611 (to S.Y.).

References

Agirman, G., Broix, L., & Nguyen, L. (2017). Cerebral cortex development: An outside-in perspective. *FEBS Letters, 591*(24), 3978-3992. doi:10.1002/1873-3468.12924

Allison, A. C. (2005). Mechanisms of action of mycophenolate mofetil. *Lupus, 14 Suppl 1*, 2. doi:10.1191/0961203305lu2109oa

An, S., Kumar, R., Sheets, E. D., & Benkovic, S. J. (2008). Reversible compartmentalization of *de novo* purine biosynthetic complexes in living cells. *Science, 320*(5872), 103-106. doi:10.1126/science.1152241

Andrews, M. G., Subramanian, L., & Kriegstein, A. R. (2020). mTOR signaling regulates the morphology and migration of outer radial glia in developing human cortex. *eLife, 9*, 10.7554/eLife.58737. doi:10.7554/eLife.58737

Ben-Sahra, I., Hoxhaj, G., Ricoult, S. J. H., Asara, J. M., & Manning, B. D. (2016). mTORC1 induces purine synthesis through control of the mitochondrial tetrahydrofolate cycle. *Science, 351*(6274), 728-733. doi:10.1126/science.aad0489

Bjornsson, C. S., Apostolopoulou, M., Tian, Y., & Temple, S. (2015). It takes a village: Constructing the neurogenic niche. *Developmental Cell, 32*(4), 435-446. doi: 10.1016/j.devcel.2015.01.010

Cho, H., Cargnin, F., Kim, Y., Lee, B., Kwon, R., Nam, H.,... Lee, S. (2014). Isl1 directly controls a cholinergic neuronal identity in the developing forebrain and spinal cord by forming cell type-specific complexes. *PLoS Genetics, 10*(4), e1004280. doi:10.1371/journal.pgen.1004280

Corbin, J. G., Rutlin, M., Gaiano, N., & Fishell, G. (2003). Combinatorial function of the homeodomain proteins Nkx2.1 and Gsh2 in ventral telencephalic patterning. *Development, 130*(20), 4895-4906. doi: 10.1242/dev.00717.

Corona-Rivera, J. R., Rea-Rosas, A., Santana-Ramirez, A., Acosta-Leon, J., Hernandez-Rocha, J., & Miguel-Jimenez, K. (2010). Holoprosencephaly and genitourinary anomalies in fetal methotrexate syndrome. *American Journal of Medical Genetics.Part A, 152A*(7), 1741-1746. doi:10.1002/ajmg.a.33496

Cronstein, B. N. (1997). The mechanism of action of methotrexate. *Rheumatic Diseases Clinics of North America, 23*(4), 739-755. doi:10.1016/s0889-857x(05)70358-6

Day, R. O., Kannangara, D. R. W., Stocker, S. L., Carland, J. E., Williams, K. M., & Graham, G. G. (2017). Allopurinol: Insights from studies of dose-response

relationships. *Expert Opinion on Drug Metabolism & Toxicology, 13*(4), 449-462. doi:10.1080/17425255.2017.1269745

Di Virgilio, F., & Adinolfi, E. (2017). Extracellular purines, purinergic receptors and tumor growth. *Oncogene, 36*(3), 293-303. doi:10.1038/onc.2016.206

Dutto, I., Gerhards, J., Herrera, A., Souckova, O., Skopova, V., Smak, J. A.,... Stracker, T. H. (2022). Pathway-specific effects of ADSL deficiency on neurodevelopment. *eLife, 11*, 10.7554/eLife.70518. doi:10.7554/eLife.70518

Emmanuel, N., Ragunathan, S., Shan, Q., Wang, F., Giannakou, A., Huser, N.,... Unsal-Kacmaz, K. (2017). Purine nucleotide availability regulates mTORC1 activity through the rheb GTPase. *Cell Reports, 19*(13), 2665-2680. doi: 10.1016/j.celrep.2017.05.043.

Englund, C., Fink, A., Lau, C., Pham, D., Daza, R. A. M., Bulfone, A.,... Hevner, R. F. (2005). Pax6, Tbr2, and Tbr1 are expressed sequentially by radial glia, intermediate progenitor cells, and postmitotic neurons in developing neocortex. *The Journal of Neuroscience : The Official Journal of the Society for Neuroscience, 25*(1), 247-251. doi: 10.1523/JNEUROSCI.2899-04.2005.

Evans, G. B., Tyler, P. C., & Schramm, V. L. (2018). Immucillins in infectious diseases. *ACS Infectious Diseases, 4*(2), 107-117. doi:10.1021/acsinfecdis.7b00172

French, J. B., Jones, S. A., Deng, H., Pedley, A. M., Kim, D., Chan, C. Y.,... Benkovic, S. J. (2016). Spatial colocalization and functional link of purinosomes with mitochondria. *Science, 351*(6274), 733-737. doi:10.1126/science.aac6054

Hoxhaj, G., Hughes-Hallett, J., Timson, R. C., Ilagan, E., Yuan, M., Asara, J. M.,... Manning, B. D. (2017). The mTORC1 signaling network senses changes in

cellular purine nucleotide levels. *Cell Reports, 21*(5), 1331-1346. doi: 10.1016/j.celrep.2017.10.029.

Huang, Z., Xie, N., Illes, P., Di Virgilio, F., Ulrich, H., Semyanov, A.,... Tang, Y. (2021). From purines to purinergic signalling: Molecular functions and human diseases. *Signal Transduction and Targeted Therapy, 6*(1), 162. doi:10.1038/s41392-021-00553-z

Jurecka, A. (2009). Inborn errors of purine and pyrimidine metabolism. *Journal of Inherited Metabolic Disease, 32*(2), 247-263. doi:10.1007/s10545-009-1094-z

Jurecka, A., Zikanova, M., Kmoch, S., & Tylki-Szymanska, A. (2015). Adenylosuccinate lyase deficiency. *Journal of Inherited Metabolic Disease, 38*(2), 231-242. doi:10.1007/s10545-014-9755-y

Ka, M., Condorelli, G., Woodgett, J. R., & Kim, W. (2014). mTOR regulates brain morphogenesis by mediating GSK3 signaling. *Development, 141*(21), 4076-4086. doi:10.1242/dev.108282

Komabayashi-Suzuki, M., Yamanishi, E., Watanabe, C., Okamura, M., Tabata, H., Iwai, R.,... Mizutani, K. (2019). Spatiotemporally dependent vascularization is differently utilized among neural progenitor subtypes during neocortical development. *Cell Reports, 29*(5), 1113-1129.e5. doi: 10.1016/j.celrep.2019.09.048.

Lavdas, A. A., Grigoriou, M., Pachnis, V., & Parnavelas, J. G. (1999). The medial ganglionic eminence gives rise to a population of early neurons in the developing cerebral cortex. *The Journal of Neuroscience, 19*(18), 7881-7888. doi: 10.1523/JNEUROSCI.19-18-07881.1999.

Lesch, M., & Nyhan, W. L. (1964). A familial disorder of uric acid metabolism and

central nervous system function. *The American Journal of Medicine, 36*, 561-570. doi: 10.1016/0002-9343(64)90104-4

Lin, J. H., Takano, T., Arcuino, G., Wang, X., Hu, F., Darzynkiewicz, Z.,... Nedergaard, M. (2007). Purinergic signaling regulates neural progenitor cell expansion and neurogenesis. *Developmental Biology, 302*(1), 356-366. doi: 10.1016/j.ydbio.2006.09.017.

Marie, S., Heron, B., Bitoun, P., Timmerman, T., Van Den Berghe, G., & Vincent, M. (2004). AICA-ribosiduria: A novel, neurologically devastating inborn error of purine biosynthesis caused by mutation of ATIC. *American Journal of Human Genetics, 74*(6), 1276-1281. doi:10.1086/421475

McManus, M. F., & Golden, J. A. (2005). Neuronal migration in developmental disorders. *Journal of Child Neurology, 20*(4), 280-286. doi:10.1177/08830738050200040301

Morita, M., Gravel, S., Chenard, V., Sikstrom, K., Zheng, L., Alain, T.,... Sonenberg, N. (2013). mTORC1 controls mitochondrial activity and biogenesis through 4E-BP-dependent translational regulation. *Cell Metabolism, 18*(5), 698-711. doi:10.1016/j.cmet.2013.10.001

Pareek, V., Pedley, A. M., & Benkovic, S. J. (2021). Human *de novo* purine biosynthesis. *Critical Reviews in Biochemistry and Molecular Biology, 56*(1), 1-16. doi:10.1080/10409238.2020.1832438

Pareek, V., Tian, H., Winograd, N., & Benkovic, S. J. (2020). Metabolomics and mass spectrometry imaging reveal channeled *de novo* purine synthesis in cells. *Science, 368*(6488), 283-290. doi:10.1126/science.aaz6465

Pedley, A. M., & Benkovic, S. J. (2017). A new view into the regulation of purine

metabolism: The purinosome. *Trends in Biochemical Sciences, 42*(2), 141-154. doi: 10.1016/j.tibs.2016.09.009.

Pelet, A., Skopova, V., Steuerwald, U., Baresova, V., Zarhrate, M., Plaza, J.,... Zikanova, M. (2019). PAICS deficiency, a new defect of *de novo* purine synthesis resulting in multiple congenital anomalies and fatal outcome. *Human Molecular Genetics, 28*(22), 3805-3814. doi:10.1093/hmg/ddz237

Seidahmed, M. Z., Shaheed, M. M., Abdulbasit, O. B., Al Dohami, H., Babiker, M., Abdullah, M. A., & Abomelha, A. M. (2006). A case of methotrexate embryopathy with holoprosencephaly, expanding the phenotype. *Birth Defects Research.Part A, Clinical and Molecular Teratology, 76*(2), 138-142. doi:10.1002/bdra.20199

Szwed, A., Kim, E., & Jacinto, E. (2021). Regulation and metabolic functions of mTORC1 and mTORC2. *Physiological Reviews, 101*(3), 1371-1426. doi:10.1152/physrev.00026.2020

Tarkowski, B., Kuchcinska, K., Blazejczyk, M., & Jaworski, J. (2019). Pathological mTOR mutations impact cortical development. *Human Molecular Genetics, 28*(13), 2107-2119. doi:10.1093/hmg/ddz042

Torres, R. J., & Puig, J. G. (2007). Hypoxanthine-guanine phosophoribosyltransferase (HPRT) deficiency: Lesch-nyhan syndrome. *Orphanet Journal of Rare Diseases, 2*, 48-48. doi: 10.1186/1750-1172-2-48

Visser, J. E., Bar, P. R., & Jinnah, H. A. (2000). Lesch-nyhan disease and the basal ganglia. *Brain Research.Brain Research Reviews, 32*(2-3), 449-475. doi: 10.1016/s0165-0173(99)00094-6

Yacubova, E., & Komuro, H. (2003). Cellular and molecular mechanisms of cerebellar granule cell migration. *Cell Biochemistry and Biophysics, 37*(3), 213-234.

doi:10.1385/cbb:37:3:213

Yamada, S., Mizukoshi, T., Tokunaga, A., & Sakakibara, S. (2022). Inka2, a novel Pak4 inhibitor, regulates actin dynamics in neuronal development. *PLoS Genetics, 18*(10), e1010438. doi:10.1371/journal.pgen.1010438

Yamada, S., & Sakakibara, S. (2018). Expression profile of the STAND protein Nwd1 in the developing and mature mouse central nervous system. *The Journal of Comparative Neurology, 526*(13), 2099-2114. doi:10.1002/cne.24495

Yamada, S., Sato, A., Ishihara, N., Akiyama, H., & Sakakibara, S. (2021). Drp1 SUMO/deSUMOylation by Senp5 isoforms influences ER tubulation and mitochondrial dynamics to regulate brain development. *iScience, 24*(12), 103484. doi:10.1016/j.isci.2021.103484

Yamada, S., Sato, A., & Sakakibara, S. (2020). Nwd1 regulates neuronal differentiation and migration through purinosome formation in the developing cerebral cortex. *iScience, 23*(5), 101058. doi: 10.1016/j.isci.2020.101058

Yamasaki, T., Kawaji, K., Ono, K., Bito, H., Hirano, T., Osumi, N., & Kengaku, M. (2001). Pax6 regulates granule cell polarization during parallel fiber formation in the developing cerebellum. *Development, 128*(16), 3133-3144. doi:10.1242/dev.128.16.3133

Yin, J., Ren, W., Huang, X., Deng, J., Li, T., & Yin, Y. (2018). Potential mechanisms connecting purine metabolism and cancer therapy. *Frontiers in Immunology, 9*, 1697. doi:10.3389/fimmu.2018.01697

Yumoto, T., Nakadate, K., Nakamura, Y., Sugitani, Y., Sugitani-Yoshida, R., Ueda, S., & Sakakibara, S. (2013). Radmis, a novel mitotic spindle protein that functions in cell division of neural progenitors. *PloS One, 8*(11), e79895.

doi:10.1371/journal.pone.0079895

Yun, K., Potter, S., & Rubenstein, J. L. (2001). Gsh2 and Pax6 play complementary roles in dorsoventral patterning of the mammalian telencephalon. *Development, 128*(2), 193-205. doi:10.1242/dev.128.2.193

Figure legends

Figure 1 De novo and salvage purine synthesis pathways and developmental expression of the enzymes catalyzing each of them in the nervous system

(A) Metabolic diagram of *de novo* (PAICS, FGAMS) and salvage (HGPRT) purine synthesis pathways in mammals. Enzymes involved in the *de novo* and salvage pathways are represented by yellow and green boxes, respectively. The route in blue represents the folate biosynthesis pathway, which is essential for substrate production of *de novo* purine synthesis. Red boxes indicate the inhibitors used in this study. (B and C) PAICS, FGAMS, and HGPRT expression detected by Westernblotting. (B) Developmental changes in the expression of each enzyme in brain lysates prepared from different developmental stages (E10.5–Adult). (C) Expression of each enzyme and Pax6 in te primary cultured neural stem/progenitor cells (NSPCs) or cortical neurons (PCNs). NSPCs and PCNs isolated from the embryonic cerebral cortex (ctx) or cerebellum (cbl) cultured for 10 days *in vitro*. α-tubulin was used as protein loading control (bottom panels). PRPP, 5-phosphoribosyl-1-pyrophosphate; PPAT, phosphoribosyl pyrophosphate amidotransferase; 5-PRA, 5-phosphoribosylamine; GART, phosphoribosylglycinamide formyltransferase; GAR, glycinamide ribonucleotide; FGAR, formylglycinamide ribonucleotide; FGAMS, formylglycin-amidine ribonucleotide synthase; FGAM, formylglycinamidine ribonucleotide; AIR,

aminoimidazole ribonucleotide; PAICS, phosphoribosylaminoimidazole succinocarboxamide synthetase; CAIR, 4-carboxy-5- aminoimidazole ribonucleotide; SAICAR, 4-(N-succinylcarboxamide)-5-aminoimidazole ribonucleotide; ADSL, adenylosuccinate lyase; AICAR, aminoimidazole-4-carboxamide ribonucleotide; FAICAR, formylaminoimidazole-4- carboxamide ribonucleotide; ATIC, 5-aminoimidazole-4-carboxamide ribonucleotide formyltransferase inosine monophosphate cyclohydrolase; DHF, dihydrofolate; DHFR, dihydrofolate reductase; THF, tetrahydrofolic acid; HGPRT, hypoxanthine-guanine phosphoribosyltransferase; APRT, adenine phosphoribosyltransferase; IMP, inosine monophosphate; IMPDH, inosine monophosphate dehydrogenase; XMP, xanthosine monophosphate; GMP, guanosine monophosphate; SAMP, adenylosuccinate; AMP, adenosine monophosphate; PNP, purine nucleoside phosphorylase; XO, xanthine oxidase; MMF, mycophenolate mofetil; MTX, methotrexate; Forodesine, forodesine hydrochloride.

Figure 2 Expression profile of purine synthesis enzymes in the developing cerebral cortex and cerebellum

(A–R) Immunostaining with anti-PAICS (A, D, G, J, M, P), anti-FGAMS (B, E, H, K, N, Q), or anti-HGPRT (C, F, I, L, O, R) antibodies in developmental ctx and cbl. Frozen sections of E13.5 ctx (A–C), E18.5 ctx (D–F), E18.5 cbl (G–I), P0 ctx (J–L), P0 cbl (M–O), and adult ctx (P–R) showing the distribution of PAICS, FGAMS, HGPRT-positive cells. Arrows indicate the HGPRT expression in EGL. (S) Representative confocal image of the E13.5 cerebral cortex double immunostained with the anti-CD31 (green) and anti-HGPRT (red) antibodies. Inset shows a higher magnification of $CD31^+$ $HGPRT^+$ endothelial cells. CP, cortical plate; VZ, ventricular zone; SVZ, subventricular

zone; EGL, external granule cell layer; GL, internal granule cell layer; MZ, marginal zone; I, cortical layer I; II/III, cortical layers II and III. Scale bars, 100 μm in (A–R); 50 μm in (S).

Figure 3 Inhibition of *de novo* purine pathway disturbs NSPC proliferation *in vitro*

(A–D) Primary cultured NSPCs from the E12.5 telencephalon were treated for 48 h with PBS or DMSO as control (A), forodesine (0.1, 1, 5 μM) (B), or mycophenolate mofetil (MMF) (1, 5 μM) (C), followed by BrdU labeling for 24 h. NSPCs were immunostained with anti-Nestin (green) and anti-BrdU (red) antibodies. (D) Quantified comparison of the number of the $BrdU^+$ $Nestin^+$ cells to total $Nestin^+$ cells. ns, not significant; ***$p < 0.001$, chi-square tests with Holm–Bonferroni correction. control PBS, n = 326; control DMSO, n = 346; forodesine 0.1 μM, n = 435; forodesine 1 μM, n = 283; forodesine 5 μM, n = 310; MMF 1 μM, n = 114; MMF 5 μM, n = 72.

(E–G) Primary cultured NSPCs were electroporated with control shRNA (E) or PAICS shRNAs (#1 or #3) (F) together with EGFP-expression plasmid (green), followed by labeling with BrdU (red) for 24 h. Arrowheads indicate GFP^+ $BrdU^+$ proliferating NSPCs. The arrow indicates $EGFP^+$ but $BrdU^-$ cells. (G) The numbers of GFP^+ $BrdU^+$ cells were compared to the total GFP^+ cells using the chi-square tests with Holm–Bonferroni correction. ns, not significant; ***$p < 0.001$. control shRNA, n = 100; PAICS shRNA#1, n = 100; PAICS shRNA#3, n = 100. Scale bars, 50 μm.

Figure 4 The development of the cerebellum is cooperatively regulated by both purine synthesis pathways

(A–D) Confocal images of the E18.5 cerebellum stained with the Ki67 (green) and BrdU (red). Control DMSO (A), forodesine (B), MMF (C), or methotrexate (MTX) (D) was administered at E16.5, followed by labeling with BrdU at E17.5, and the cerebellum was analyzed at E18.5. (A'–D') Higher magnification of A–D. (E) Quantified comparison of the percentage of Ki67- BrdU+ cells to total $BrdU^+$ cells in GL at E18.5.

(F–H) Confocal images of the P6 cerebellum stained with the Ki67 (green) and BrdU (red). Control DMSO (F), forodesine (G), or MMF (H) was administered to P2 pups, followed by BrdU labeling at P4, and the cerebellum was immunostained at P6. (F'–H') Higher magnification of F–H. (I) Quantified comparison of the percentage of $Ki67^-$ $BrdU^+$ cells to the total $BrdU^+$ cells in the GL at P6. Data are presented as means ± SEM. *$p < 0.05$, **$p < 0.01$, Welch's *t*-test followed by Holm–Bonferroni correction. EGL, external granule cell layer; GL, internal granule cell layer. Scale bars, 100 μm.

Figure 5 Formation of the cerebral cortex mainly depends on the *de novo* purine pathway

(A–H) E12.5 embryos were treated with control DMSO (A, E), forodesine (B, F), or MMF (C, G), followed by BrdU labeling, and analyzed at E14.5. Horizontal frozen sections were immunostained with anti-BrdU antibody (red) (A–C) or p-Histone H3 (pH3) antibody (red) (E–H). Arrows in (G) indicate $pH3^-$ VZ areas. (D) Quantification of the percentage of $BrdU^+$ cells distribution in each layer (CP, IZ, SVZ/VZ). (H) Number of $pH3^+$ cells/500 μm width of the VZ region. Data are presented as means ± SEM. ns, not significant, *$p < 0.05$, **$p < 0.01$, ***$p < 0.001$, Welch's *t*-test followed by Holm–Bonferroni correction.

(I–Q) Immunostaining of PAICS (I–K), FGAMS (L–N), and HGPRT (O–Q) in the VZ/SVZ area of E14.5 embryos treated with DMSO (I, L, O), forodesine (J, M, P), or MMF (K, N, Q). Nuclei were stained with Hoechst dye (blue).

MZ, marginal zone; CP, cortical plate; IZ, intermediate zone; SVZ/VZ, subventricular zone/ventricular zone. Scale bars, 100 μm in (A–C) and (E–G); 20 μm in (I–Q).

Figure 6 Embryonic brain malformations induced by inhibiting the *de novo* pathway

(A–F) Horizontal frozen sections of E12.5 brains. DMSO (A'), MMF (B), forodesine (C), MTX (D'), allopurinol (E'), or MTX plus Allopurinol (F) were successively administered at E9.5–E11.5 and brains were harvested at E12.5. Nuclei were stained with Hoechst dye (cyan). (A'–F') Magnified views of the forebrain of A–F. lv, lateral ventricles; 3v, 3rd ventricle. Scale bars, 500 μm in (A–F), 100 μm in (A'–F').

Figure 7 *De novo* pathway inhibition causes forebrain-specific malformation

(A–T) Control DMSO (A, E, I, M, Q, U, W), MMF (B, F, J, N, R, V, X), forodesine (C, G, K, O, S), or allopurinol (D, H, L, P, T) was administered to pregnant mice between E9.5–11.5 and analyzed at E12.5. Horizontal frozen sections were immunostained with antibodies to cleaved-caspase3 (red) (A–D), Pax6 (green)/DCX (red) (E–H), Tbr2 (green) (I–L), Ki67 (red) (M–P), pH3 (green) (Q–T), Nestin (green) (U, V), or GSH2 (green) (W, X). The forebrain region treated with MMF was divided by dotted lines into area 1 ($Pax6^{-}$ $GSH2^{+}$) and area 2 ($Pax6^{+}$ $GSH2^{-}$). The asterisk in (F) denotes the expanded cortical layer filled with DCX^{+} immature neurons.

(Y and Z) Quantification of cleaved-caspase3^{+} (Y) or $pH3^{+}$ (Z) cells in the cerebral

cortex (number of cells per 500 μm width of the cortex). In MMF-treated embryos, cleaved-caspase3^{+} or pH3^{+} cells were counted in area 1 and area 2, respectively. ns, not significant, **$p < 0.01$, Welch's *t*-test followed by Holm–Bonferroni correction. Scale bars, 100 μm in (A–X). (AA) Schematic model of brain abnormalities caused by *de novo* pathway inhibition. Control (left upper panel) or MMF-treated brains (left lower panel) were cut in the horizontal (middle panels) or sagittal plane (right panels). Horizontal sections were then sliced through the orange line shown in the 3D brain (left). MMF-treated brains show a loss or hypoplasia of the rostral neocortex and a dorsal expansion of striatal GE (blue), resulting in abnormal forebrain structures. In MMF-treated embryos, the rostral neocortex (RN) containing Pax6+ VZ disappeared; instead, the GE containing GSH2^{+} VZ ectopically appeared on the dorsal surface. lv, lateral ventricles; 3v, 3rd ventricle; 4v, 4th ventricle; GE, ganglionic eminence.

Figure 8 The *de novo* purine pathway affects mTORC1/S6K/S6 signaling

(A) Immunoblot analysis of E12.5 brains treated with each inhibitor at E9.5–E11.5. Each panel shows the expression of mTOR signaling proteins (pS6K, S6K, pS6, S6, and 4E-BP1) and purine synthesis enzymes (PAICS, FGAMS, and HGPRT). The blot was reprobed with α-tubulin antibody (bottom) to examine quantitative protein loading. (B) Quantified comparison of the pS6/S6 ratio. Data are presented as means ± SEM. ns, not significant, **$p < 0.01$, Welch's *t*-test followed by Holm–Bonferroni correction. (C) Schematic diagram of the relationship between mTOR signaling and purine nucleotides.

Fig.1

A

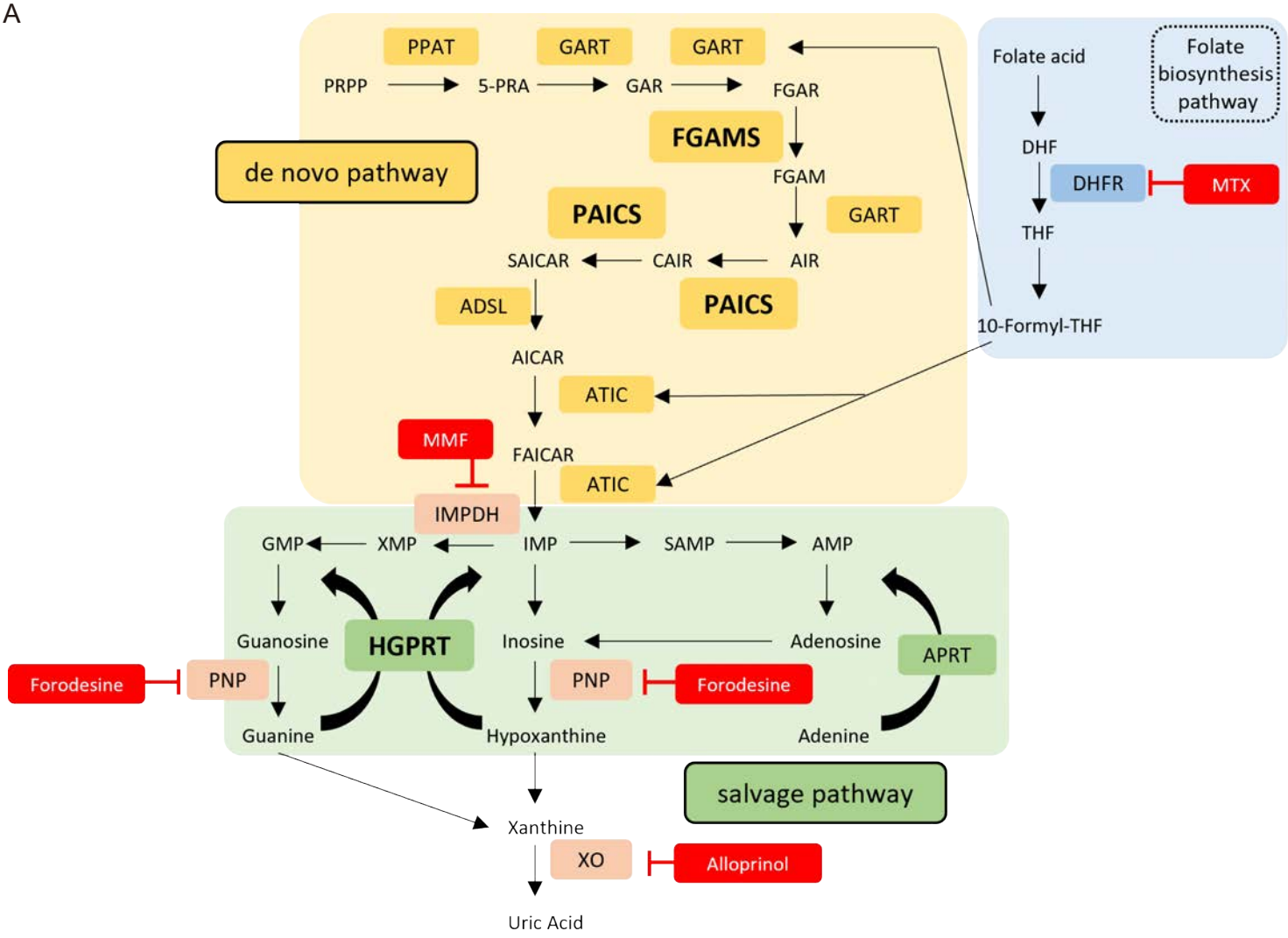
PPAT
GART
GART
PRPP
5-PRA
GAR
FGAR
FGAMS
de novo pathway
FGAM
PAICS
GART
SAICAR
CAIR
AIR
ADSL
PAICS
AICAR
ATIC
MMF
FAICAR
ATIC
IMPDH
Folate acid
Folate biosynthesis pathway
DHF
DHFR
MTX
THF
10-Formyl-THF
GMP
XMP
IMP
SAMP
AMP
Guanosine
HGPRT
Inosine
Adenosine
APRT
Forodesine
PNP
PNP
Forodesine
Guanine
Hypoxanthine
Adenine
salvage pathway
Xanthine
XO
Alloprinol
Uric Acid

B

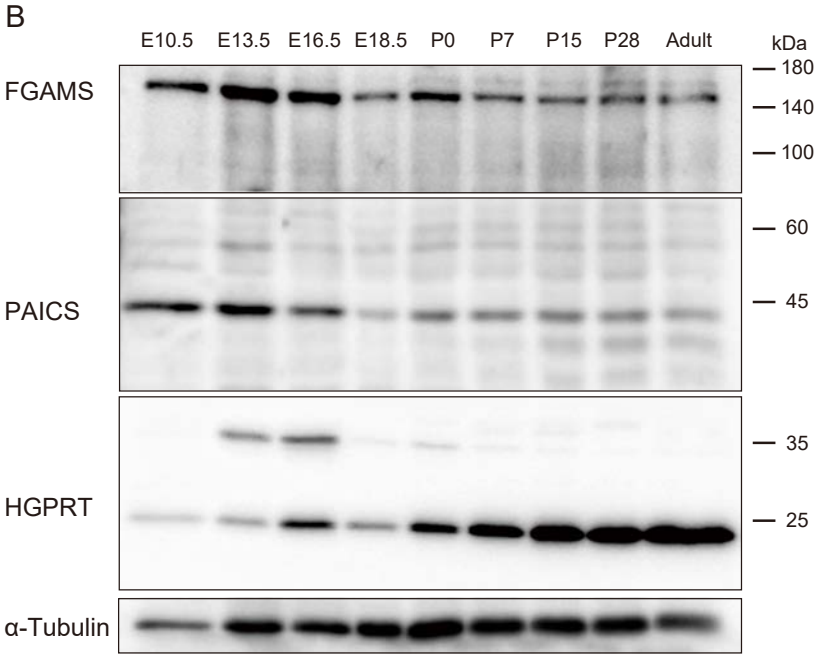
E10.5
E13.5
E16.5
E18.5
P0
P7
P15
P28
Adult
kDa
FGAMS
180
140
100
PAICS
60
45
HGPRT
35
25
α-Tubulin

C

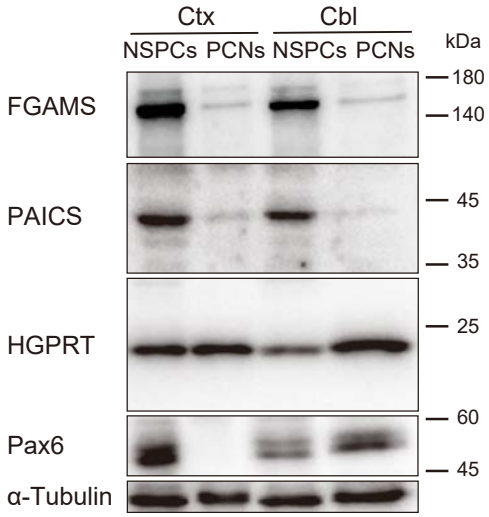
Ctx
Cbl
NSPCs
PCNs
NSPCs
PCNs
kDa
FGAMS
180
140
PAICS
45
35
HGPRT
25
Pax6
60
45
α-Tubulin

Fig.2

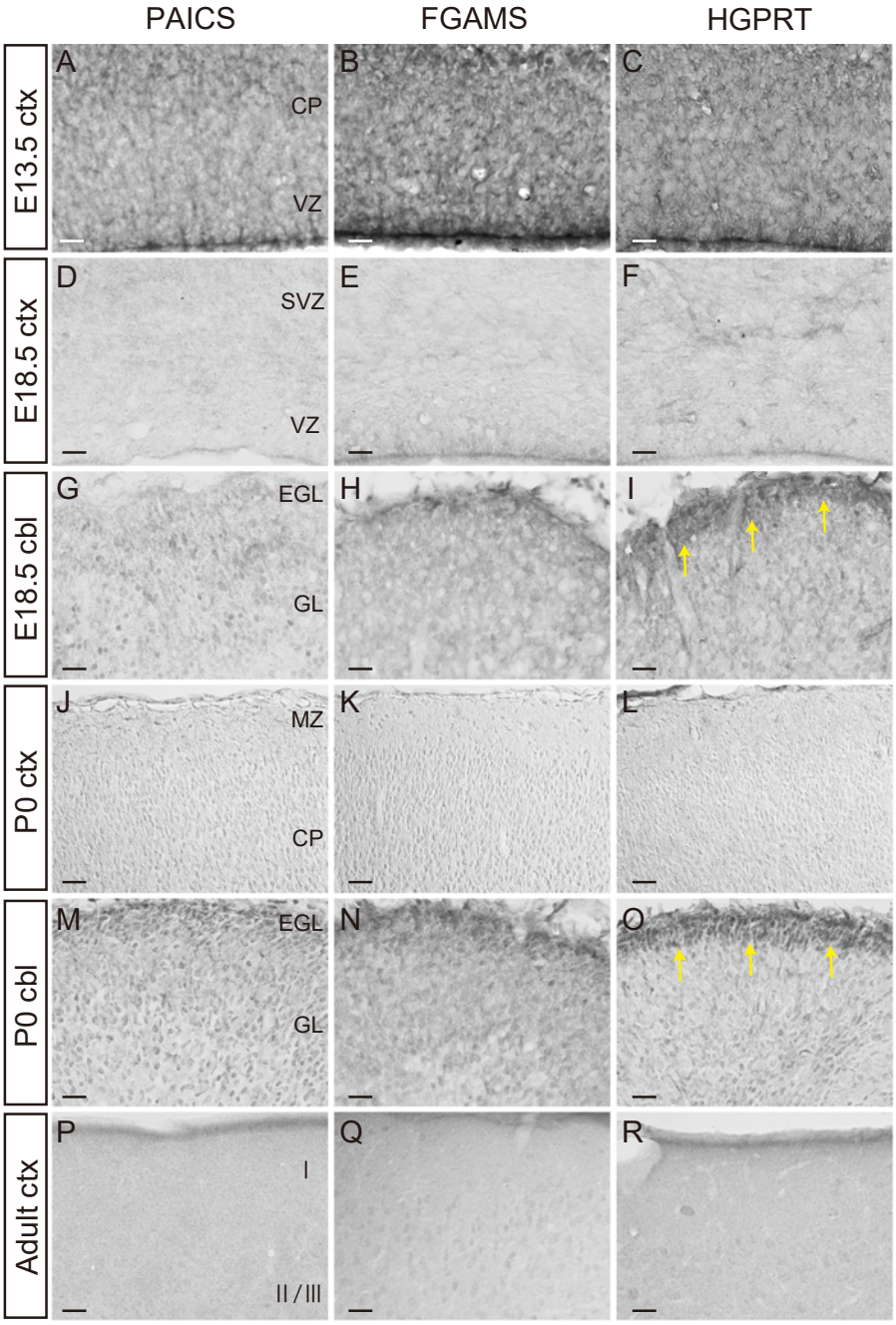
PAICS
FGAMS
HGPRT
E13.5 ctx
E18.5 ctx
E18.5 cbl
P0 ctx
P0 cbl
Adult ctx
A
B
C
CP
VZ
D
E
F
SVZ
VZ
G
H
I
EGL
GL
J
K
L
MZ
CP
M
N
O
EGL
GL
P
Q
R
I
II / III

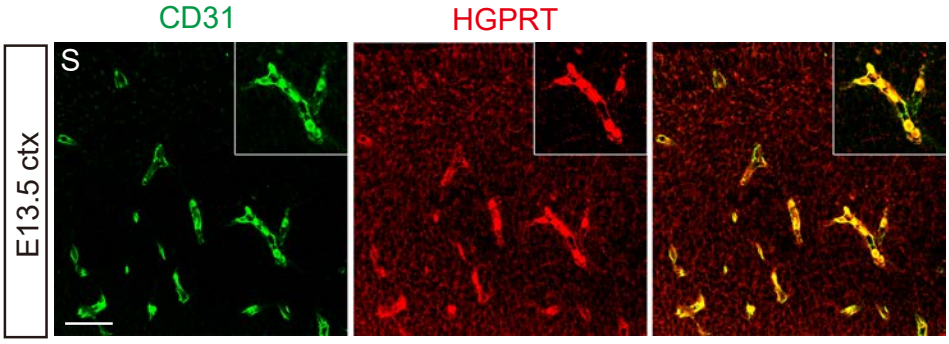
CD31
HGPRT
E13.5 ctx
S

Fig.3

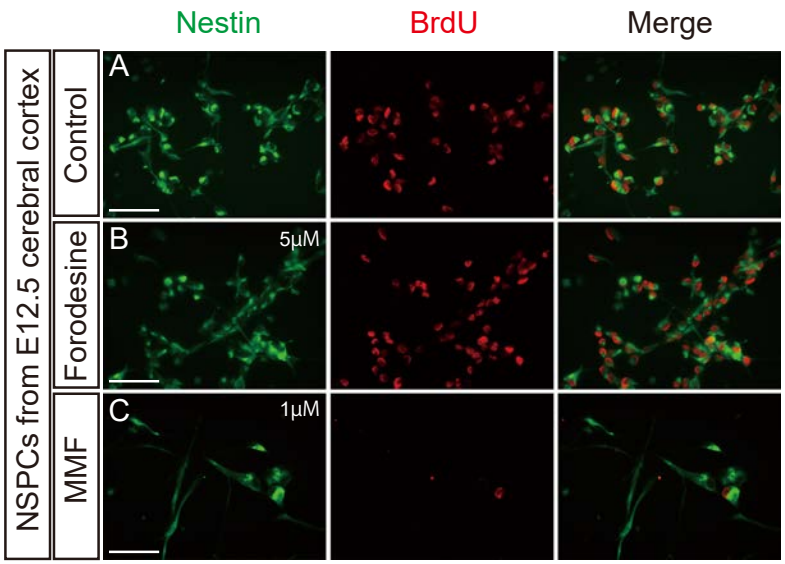
Nestin
BrdU
Merge
NSPCs from E12.5 cerebral cortex
Control
Forodesine
MMF
A
B
5μM
C
1μM

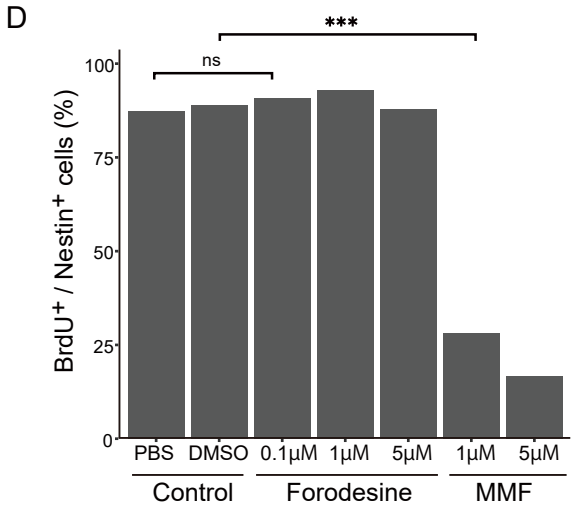
D
***
ns
100
75
50
25
0
BrdU+ / Nestin+ cells (%)
PBS
DMSO
0.1μM
1μM
5μM
1μM
5μM
Control
Forodesine
MMF

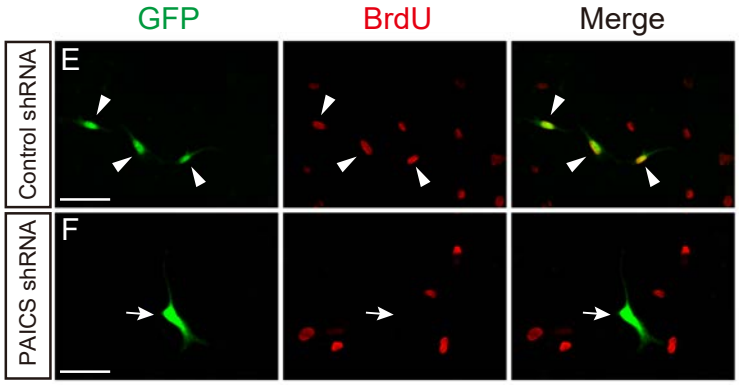
GFP
BrdU
Merge
Control shRNA
PAICS shRNA
E
F

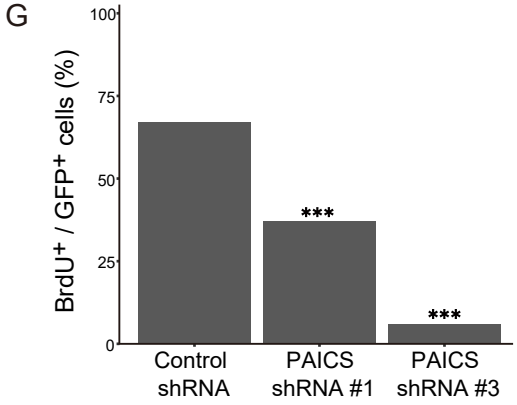
G
100
75
50
25
0
BrdU+ / GFP+ cells (%)
***
***
Control shRNA
PAICS shRNA #1
PAICS shRNA #3

Fig.4

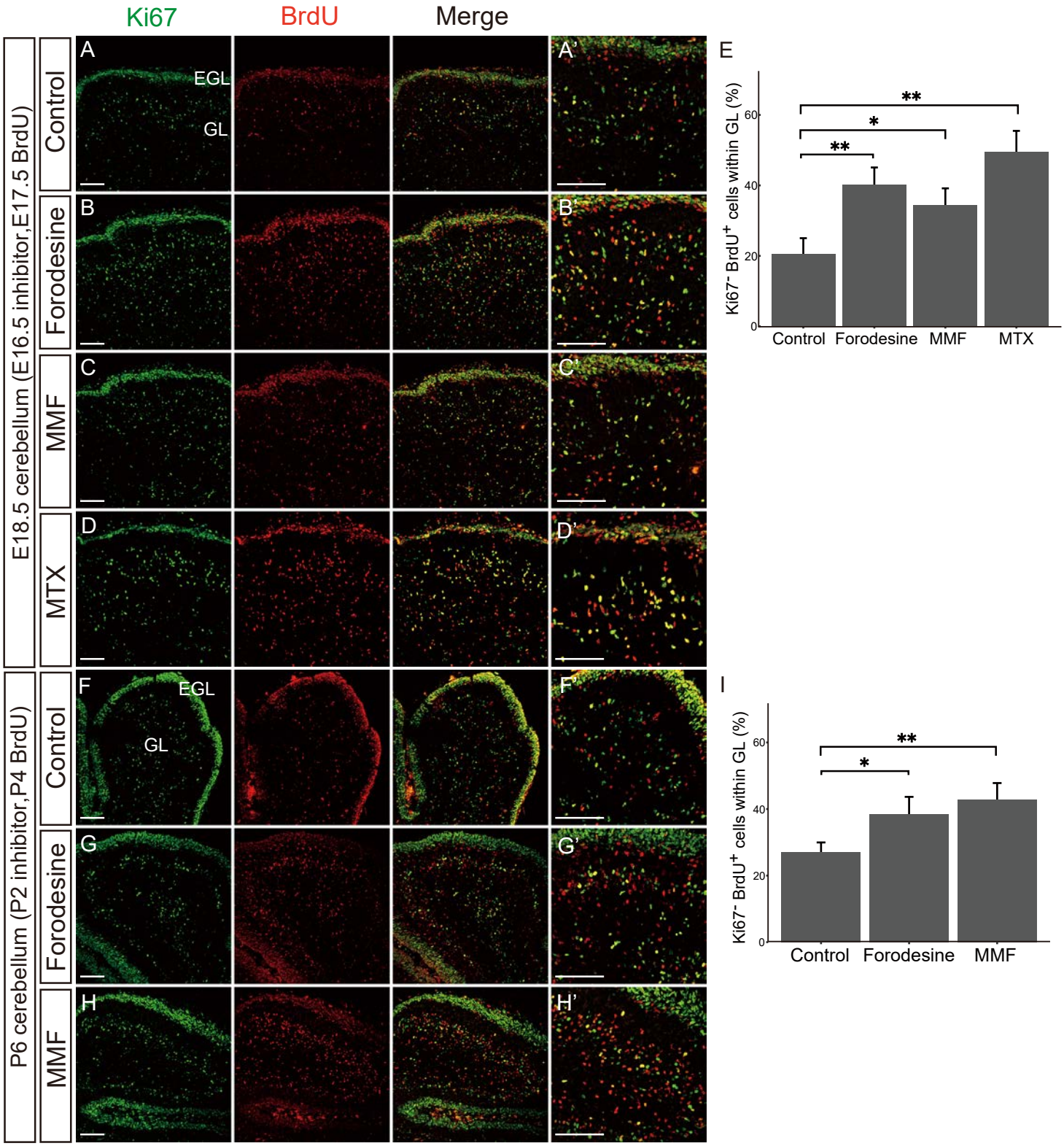
Ki67
BrdU
Merge
E18.5 cerebellum (E16.5 inhibitor,E17.5 BrdU)
Control
Forodesine
MMF
MTX
P6 cerebellum (P2 inhibitor,P4 BrdU)
Control
Forodesine
MMF
A
A'
B
B'
C
C'
D
D'
F
F'
G
G'
H
H'
EGL
GL
E
Ki67⁻ BrdU⁺ cells within GL (%)
0
20
40
60
**
*
**
Control
Forodesine
MMF
MTX
I
Ki67⁻ BrdU⁺ cells within GL (%)
0
20
40
60
**
*
Control
Forodesine
MMF

Fig.5

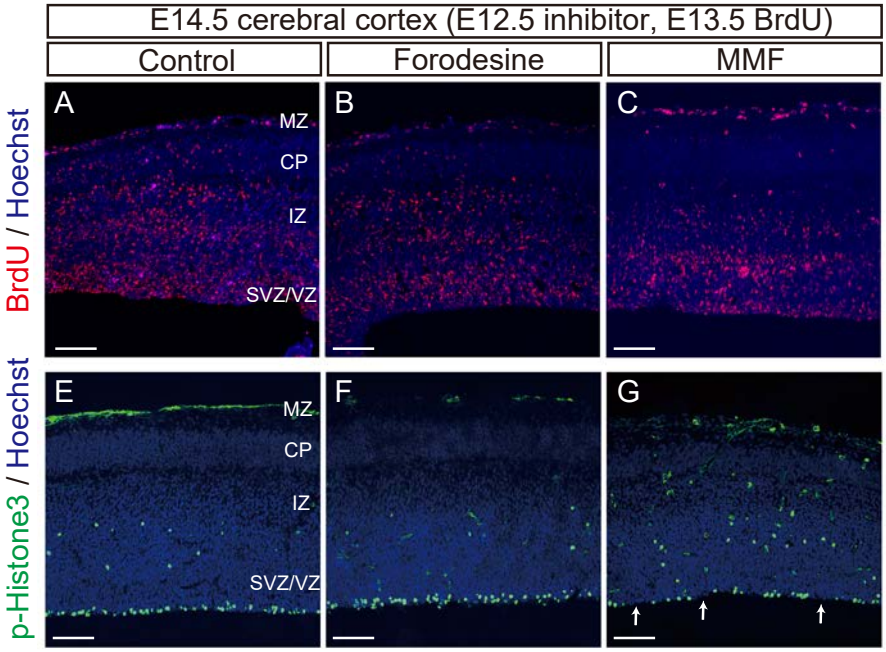
E14.5 cerebral cortex (E12.5 inhibitor, E13.5 BrdU)
Control
Forodesine
MMF
BrdU / Hoechst
p-Histone3 / Hoechst
A
B
C
E
F
G
MZ
CP
IZ
SVZ/VZ

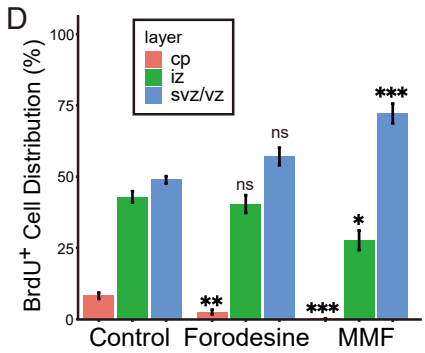
D
BrdU+ Cell Distribution (%)
layer
cp
iz
svz/vz
100
75
50
25
0
**
***
ns
ns
*
***
Control
Forodesine
MMF

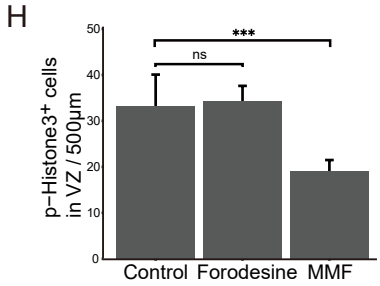
H
p−Histone3+ cells in VZ / 500μm
50
40
30
20
10
0
***
ns
Control
Forodesine
MMF

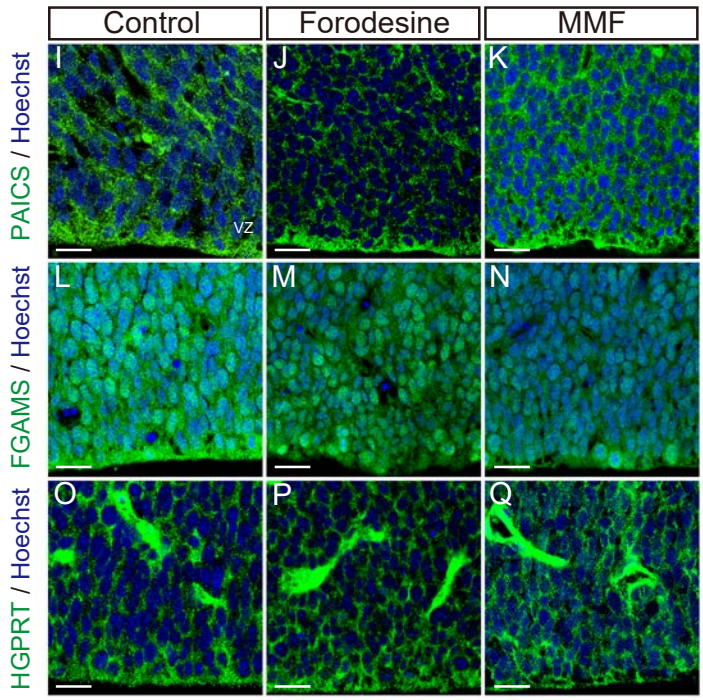
Control
Forodesine
MMF
PAICS / Hoechst
FGAMS / Hoechst
HGPRT / Hoechst
I
J
K
L
M
N
O
P
Q
VZ

Fig.6

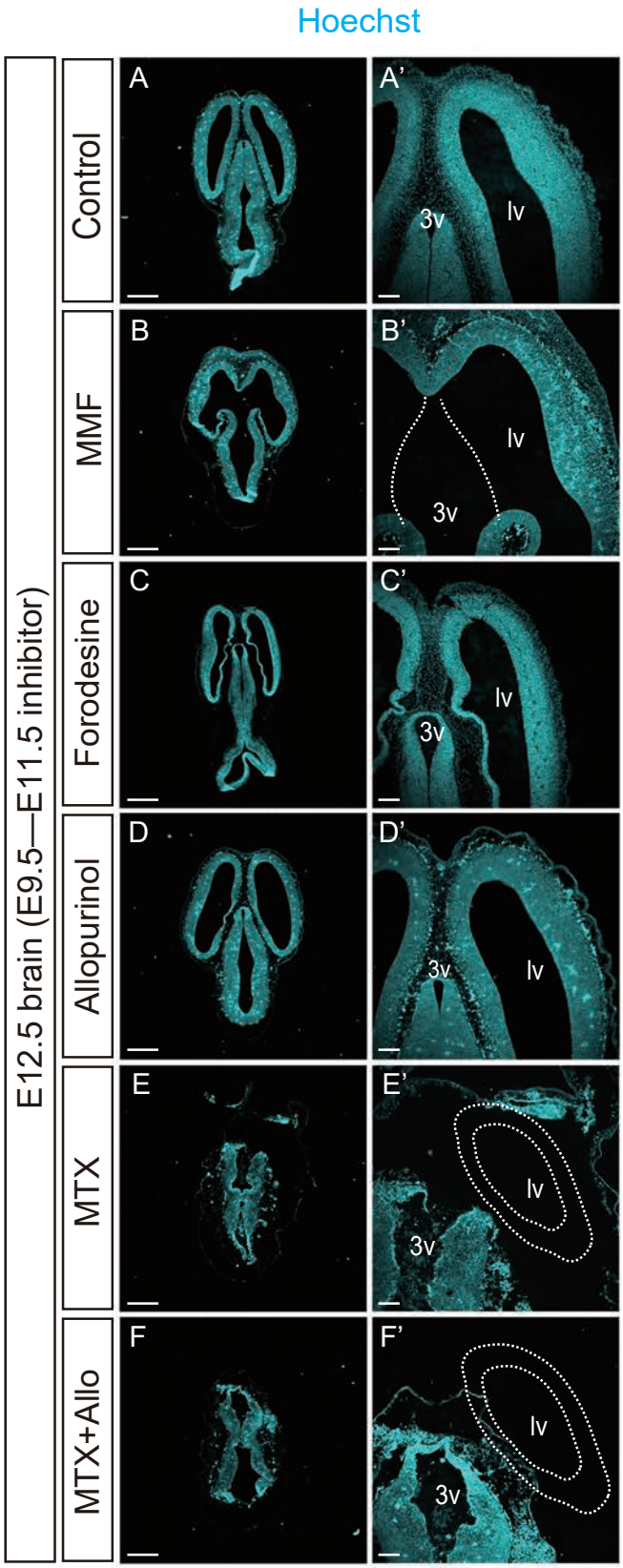
Hoechst
E12.5 brain (E9.5—E11.5 inhibitor)
Control
MMF
Forodesine
Allopurinol
MTX
MTX+Allo
A
A'
B
B'
C
C'
D
D'
E
E'
F
F'
3v
lv

Fig.7

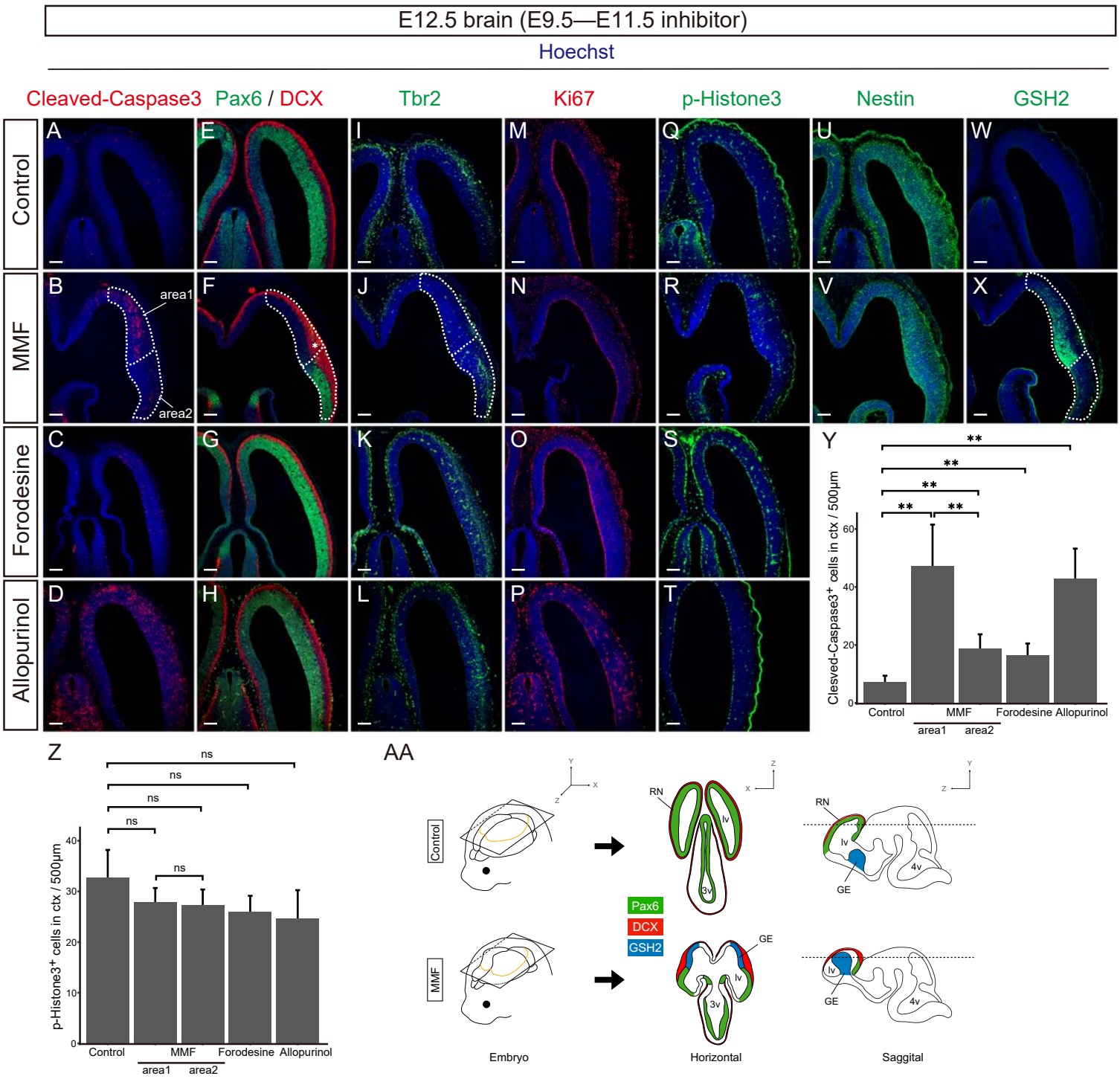
E12.5 brain (E9.5—E11.5 inhibitor)
Hoechst
Cleaved-Caspase3
Pax6 / DCX
Tbr2
Ki67
p-Histone3
Nestin
GSH2
Control
MMF
Forodesine
Allopurinol
area1
area2
Y
Clesved-Caspase3+ cells in ctx / 500μm
Control
MMF
Forodesine
Allopurinol
Z
p-Histone3+ cells in ctx / 500μm
ns
AA
Control
MMF
Pax6
DCX
GSH2
RN
lv
3v
GE
4v
Embryo
Horizontal
Saggital

Fig.8

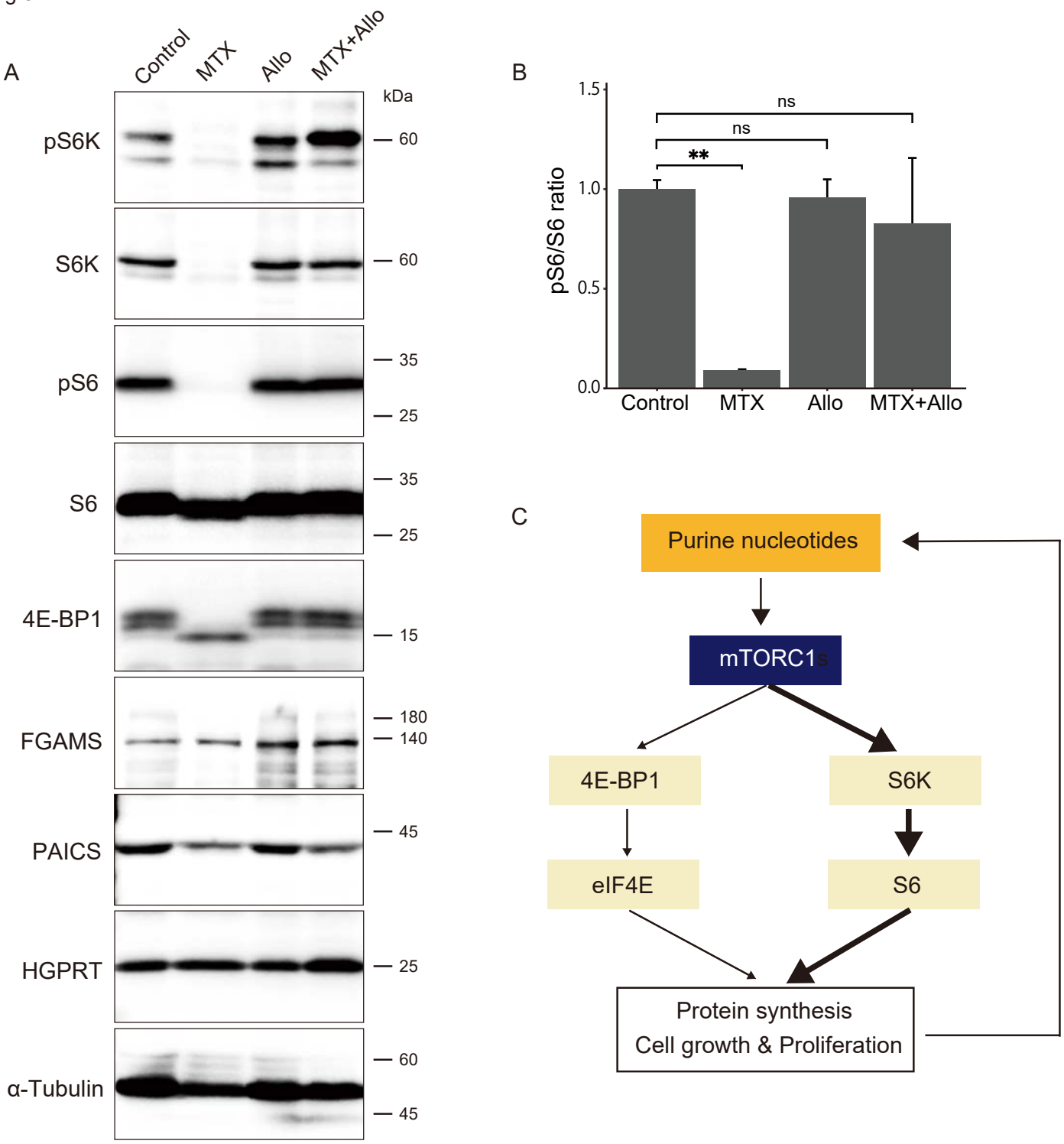
A
Control
MTX
Allo
MTX+Allo
kDa
pS6K
60
S6K
60
pS6
35
25
S6
35
25
4E-BP1
15
FGAMS
180
140
PAICS
45
HGPRT
25
α-Tubulin
60
45
B
pS6/S6 ratio
1.5
1.0
0.5
0.0
ns
ns
**
Control
MTX
Allo
MTX+Allo
C
Purine nucleotides
mTORC1s
4E-BP1
S6K
eIF4E
S6
Protein synthesis
Cell growth & Proliferation